Kang et al. Int J Concr Struct Mater (2024) 18:16
https://doi.org/10.1186/s40069-023-00659-4

International Journal of Concrete Structures and Materials

RESEARCH

Open Access

Analysis of the Strength of Different Minerals-Modified MPC Based on Mathematical Models

Qi Kang[1*], Jingxin Bao[2], Ran Li[1], Yingying Zuo[1], Yanxia Ye[1*] and Hua Huang[3]

Abstract

The study discussed the effects of different mineral incorporations and the curing time on the strength of modified magnesium phosphate cement (MPC) mortars through mechanical tests, mathematical model analysis and microstructure characterization. Fly ash (FA), silica fume (SF), and metakaolin (MK), which exhibit excellent durability and bonding properties, were used to modify the MPC. A quantitative relationship was established between the strength of modified MPC mortars and the mineral incorporation and curing time. First, the strength of each mineral-modified MPC mortar cured in air with different mineral incorporations and curing durations was evaluated. The strengths of MPC mortars containing 10% fly ash, 15% silica fume, and 10% metakaolin—which perform best in their incorporations—were compared to analyze the function of the three minerals. To establish the relationship between strength and mineral incorporation and curing time, three mathematical models, linear model, general nonlinear model, and data distribution shape nonlinear model (DDSNM), are commonly used for material property analysis based on statistics. DDSNM best describes the trend of strength change among the three models and the error is small for three minerals. Based on DDSNM, the influence of various minerals on the strength of MPC mortar was quantitatively evaluated by calculating the variable partial derivatives, and verified by scanning electron microscopy and X-ray diffraction. MK performs the best in improving the flexural strength performance of MPC, while SF performs the best in the compressive strength. FA-MPC has low sensitivity to dosage fluctuations and is easy to prepare.

Keywords Magnesium phosphate cement mortar (MPC), Mineral modified materials, Mechanical test, Mathematical strength model, Microstructure characterization

Journal information: ISSN 1976-0485 / eISSN 2234-1315.

*Correspondence:
Qi Kang
kangqi0816@outlook.com
Yanxia Ye
yeyanxia@chd.edu.cn
[1] School of Civil Engineering, Chang'an University, Xi'an 710061, China
[2] Chang'an Dublin International College of Transportation, Chang'an University, Xi'an 710061, China
[3] School of Civil & Architecture Engineering, Xi'an Technological University, Xi'an 710061, China

1 Introduction

With the increasing global warming trend and urgent demand for energy, magnesium phosphate cement (MPC), a new green cementitious material, has gradually become a priority candidate for the building industry (Ruan, 2022). MPC is progressively being adopted to reduce carbon emissions and safeguard the ecosystem against global warming (Chau et al., 2011) due to its excellent performance in mechanical properties and CO_2 absorption (Walling & Provis, 2016). With features of fast hardening, high early strength, high adhesive strength, low drying shrinkage, and easy construction in a low-temperature environment (Fang et al., 2023; Yang et al., 2014), MPC materials have been used to rapidly repair concrete structures (El-Jazairi, 1982; Wang et al., 2023).

Despite rapid development and wide application, the prepared MPC-based material cured in water showed worse mechanical performance and durability than the material cured in the air (Bai et al., 2023; Jiang et al., 2019). In order to address this problem, Liao (Liao et al., 2017) replaced low-grade fly ashes (LGFA) in varying volumes for MPC material. He discovered that the higher the quantity of LGFA, the lower the strength of LGFA, and the higher the water-resistance ability. Furthermore, Muhammad Riaz Ahmad (Ahmad et al., 2019) incorporated ultrafine fly ash (FA) into basalt fiber-reinforced MPC and found that FA improved the mechanical properties of MPC composites such as the flexural strength and water-resistance ability. Meanwhile, because of the obvious effect of silica fume (SF) in reducing total porosity, improving strength, and enhancing water-resistance ability (Xie et al., 2020). Ma (Ma et al., 2022) systematically investigated the mechanism of the effect of SF on the early performance of MPC which was used for repairing coatings of hydraulic structures and pointed out that SF played a significant filling role in MPC and improved the denseness of the substrate. Muhammad Riaz Ahmad (Ahmad & Chen, 2018) also studied the strength change of MPC mortar with a variation of SF from 0 to 10% and found that the strength of MPC mortar increased with SF increased. Same as other minerals, metakaolin (MK) is also used to improve the water-resistance ability and dynamic strength of MPC because it can produce finer pores to make the pore structure more uniform (Runqing et al., 2023). Lv (Lv et al., 2019) conducted the strength test on water-cured MK-modified MPC paste specimens and pointed out that MK is beneficial to improve the compressive strength and water stability of MPC paste, and then Qin (Qin et al., 2020) carried out strength tests on MPC mortar with different MK contents under natural curing conditions and found that the strength gradually increased with curing time and the strength on the 28th day increased significantly with the increase of incorporation. Based on SEM and XRD microscopic research and analysis, the addition of FA, SF, and MK introduces SiO_2 particles, which adsorb other products with unreacted MgO to form more regular shaped crystals, reducing the number of structural micropores and resulting in a denser microstructure (Sun et al., 2023; Zhang et al., 2023).

Although it is known in many studies that the addition of minerals to MPC materials can enhance their related properties, there is no clear statement on which mineral materials perform better when added to MPC mortars in terms of strength. However, understanding the relationship between the strength of modified MPC mortar and the amount of mineral incorporation and the curing time is the key to improving the stability of MPC material performance in practical use. Therefore, to quantify a relationship in equations that reasonably describes the variation of the strength of modified MPC mortar with relevant variables is the basis for the promotion and application of modified MPC mortar.

When it comes to quantifying the material properties or the structure performance, mathematical methods such as machine learning and mathematical statistics are generally used in civil engineering. In terms of determining the elastic module of concrete samples, Ahmadi (Ahmadi & Kioumarsi, 2023) adopted particle swarm optimization to develop artificial neural networks. Sattarifard (Sattarifard et al., 2022) studied the impact and engineering material properties of the hybrid fiber reinforced-compacting cementitious composites by means of regression analysis and probability statistics analysis, and proposed the most appropriate statistical distribution function. Mathematical modeling methods are often used to achieve a quantitative description of the relationship between material properties and material ratios. Sergio (Huete-Hernández et al., 2021) modeled the relationship between different properties and raw material ratios based on the response surface shape to analyze the relationship between the properties of ceramic waste-filled magnesium phosphate cement and each raw material ratio by different forms of mathematical models with less error. In the same method, Yue (Yue et al., 2016) established a mathematical model to describe the rheological properties of MPC. In the application of mathematical models for material strength, Zhou (Zhou et al., 2019) used power function and linear function models to study the relationship between the compressive strength of backfilled cement slurry under different curing times and cement-to-tailing ratio and slurry concentration and further derived mathematical models for the effects of cement-to-tailing ratio and slurry concentration on strength under different curing times, which obtained better accuracy. Wael Mahmood (Mahmood et al., 2022) used a linear model, a nonlinear model, and a multiple-linear model to study the effects of multiple independent variables on the compressive strength of cement grouting sand, among which the nonlinear model was of the best performance.

In general, there are seldom methods analyzing and quantifying the concrete function of minerals in the strength of modified-MPC. In order to assess the role of minerals of fly ash (FA), silica fume (SF), and metakaolin (MK) on the mechanical performance of MPC, and build up the strength predicting model, they were selected to modify MPC mortars in this study, which generated test blocks to get their mechanical performance. The specific relationship between mineral incorporations and curing time and the strength of modified MPC mortar was then modeled using a linear model (LM), a general nonlinear model (GNM), and a data distribution-shaped nonlinear model (DDSNM) based on limited tested data. The best-performing model was then chosen to calculate the strength influence coefficient with partial differentiation. This approach allowed for a more thorough evaluation of the effects of various minerals on the strength of the modified MPC mortar. After 28 days of air-curing, the relevant data of the three mineral-modified MPC mortars were evaluated and microscopically analyzed at their optimal incorporations, and the advantages of the three mineral materials were thoroughly clarified. Through this approach, the macro-mathematical model analysis of the test results and the micro-characterization of the experimental observations were combined to investigate the effect of different mineral materials on the strength of MPC mortar, and quantitative evaluation coefficients were obtained whose accuracy was verified by the micro-results.

2 Materials and Methods

2.1 Raw Materials

In the experiment, dead burned magnesium oxide, potassium dihydrogen phosphate, natural river sand, and composite retarder (CR) composed of industrial-grade boric acid and glucose were chosen as the main raw materials (Bai et al., 2023; Ma et al., 2021), and three mineral materials, fly ash (FA), silica fume (SF) and metakaolin (MK), were taken as the modifying materials to prepare the modified MPC mortars used in the experiment, which were recorded as FA-MPC, SF-MPC, and MK-MPC. The mentioned minerals would equally replace a certain weight of magnesium oxide and potassium dihydrogen phosphate to act in the MPC mortar system. The detailed information of the material used in the test is listed in Table 1. The chemical composition of raw materials is shown in Table 2.

2.2 Samples Preparation

The curing time of five levels including 3 h, 1 day, 3 days, 7 days, and 28 days were selected. Except for the incorporation of MK was selected as 5%, 10%, and 15% in three levels, the incorporation of the remaining two minerals was selected as 5%, 10%, 15%, and 20% in four levels

Table 1 Information of raw materials

Material	Main content	Purity/level	sources	Others
Dead burned magnesium oxide	MgO	95%	Yancheng, Jiangsu province, China,	Specific surface area = 320m^2/kg Calcination temperature > 1500 ℃
Potassium dihydrogen phosphate	KH_2PO_4	> 99%	Tianjin Zhonghe Shengtai Chemical Co., Ltd	Particle size = 0.55 ~ 1 mm
Compound retarder				
Boric acid	H_3BO_3	99.9%	Jinan Xiangfeng Weiye Chemical Co., Ltd	Relative density = 1.43 Melting point = 171 ℃ Acidic aqueous solution
Glucose	$C_6H_{12}O_6$	99.9%	Henan Zhongbang Environmental Protection Technology Co., Ltd	Relative density = 1.581 Melting point = 146 ℃
Fly ash	–	First grade	Henan Yuanheng Environmental Protection Engineering Co., Ltd	–
Silica fume	–	High quality	Henan Dingnuo Purification Material Co., Ltd	–
Metakaolin	–	–	Shanxi Xingle Kaolin Co., Ltd	Particle size = 1250 mesh Whiteness > 92%

Table 2 Chemical composition of raw materials

Material	MgO	SiO_2	CaO	Al_2O3	Fe_2O_3	Na_2O	TiO_2	K_2O	Others
MgO	99.20%	0.20%	0.10%	0.10%	0.30%	–	–	–	0.01%
FA	–	54.76%	4.85%	24.56%	6.5%	–	1.85%	–	7.48%
SF	0.65%	94.8%	1.86%	0.81%	0.08%	0.45%	–	–	1.35%
MK	–	48.73%	0.12%	46.12%	0.35%	–	1.32%	0.1%	3.13%

Table 3 Mix proportion and the number of test blocks

M/P	CR (wt.%)	W/C	Sand–binder ratio	Mineral admixtures	Mineral incorporation (wt.%)	Curing time	Number of test blocks	Sum
6	3%	0.23	1	FA	5% 10% 15% 20%	3h, 1d, 3d, 7d, 28d	4×5×3=60	165
				SF			4×5×3=60	
				MK	5% 10% 15%		3×5×3=45	

to design the test and prepare the samples (Table 3). The dead burned magnesium oxide, potassium dihydrogen phosphate, compound retarder, natural river sand, mineral materials, and water were weighed first, and the solid raw materials were then added into the mixer. And the machine was started and stirred for 1 min first to make the dry raw materials stirred well, then water would be added quickly. The materials would be stirred for 30 s first at low speed, and then for 90 s at high speed until the cement mortar has good fluidity and uniformity. After the above procedure was done, the mixed material should be poured into the 40 mm×40 mm×160 mm test mold quickly and put on the cementitious sand vibrating table to vibrate and smoothed out, according to *Code for Test method of cement mortar strength (ISO method)* (The State Bureau of Quality & Technical Supervision, 2021a). The process of adding water to pour mortar into the mold should be controlled within 3 min. The schematic diagram of sample preparation procedure is shown in Fig. 1. Three samples were made for each level, and after molding, the mold could be

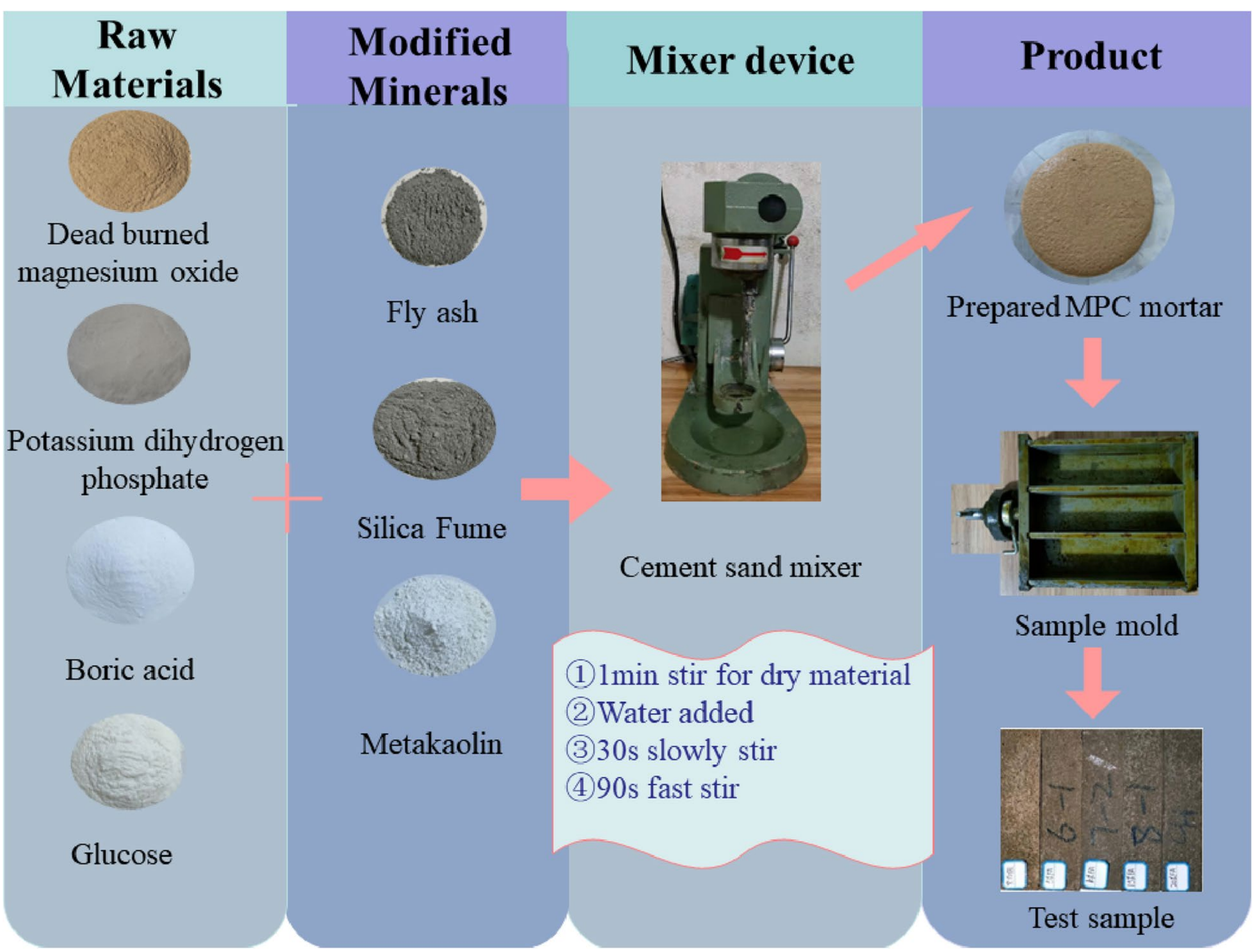

Fig. 1 Schematic diagram of sample preparation procedure

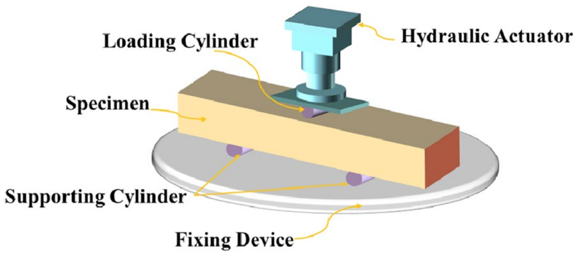

Fig. 2 Schematic diagram of flexural strength test

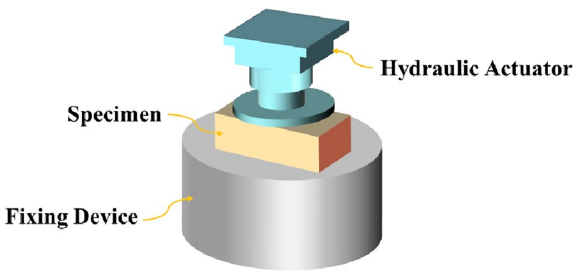

Fig. 3 Schematic diagram of compressive strength test

removed within 3 h, and then the samples would be placed in the air for natural curing with a temperature of 20 ± 2℃ and relative humidity of 50% ± 5%.

2.3 Strength Test

The flexural strength was tested by placing one side of a sample on the supporting cylinder of the testing machine (Fig. 2), and the load was applied vertically to the opposite side of the prism at a uniform rate of 50 N/s ± 10 N/s by the loading cylinder until a sample fractured (The State Bureau of Quality & Technical Supervision, 2021b). The flexural strength, σ_f, was calculated according to Eq. (1). After the completion of the flexural strength test, two semi-truncated samples were moved for the compressive strength test (The State Bureau of Quality & Technical Supervision, 2021b). The test was performed on the side of the semi-truncated prism (Fig. 3). The difference between the center of the semi-truncated prism and the press platen pressed center should be within ± 0.5 mm, and the part of the prism exposed outside the platen should be about 10 mm. The prism would be uniformly loaded at a rate of 2400 N/s ± 200 N/s during the whole loading process until damaged. The compressive strength σ_c could be calculated by Eq. (2):

$$\sigma_f = \frac{1.5F_f L}{b^3}, \tag{1}$$

$$\sigma_c = \frac{F_c}{A}, \tag{2}$$

where F_f is the load applied to the middle of the prism at fracture of the specimen (N), L is the distance between the two supporting cylinders(mm), b is the side length of the prism square section(mm), F_c is the maximum load of the damage of the semi-truncated prism(N), and A is the area of the pressed part (mm^2).

2.4 Test Results and Analysis

The strength evolutions of the three minerals modified MPC mortar samples, under different mineral incorporations, at different curing times of 3 h, 1, 3, 7, and 28 days, are shown in Figs. 4, 5, 6. It can be visually observed that the strength of modified MPC mortar is positively correlated with the curing time, while the strength of different minerals modified MPC mortar samples shows the various optimal incorporation.

The change in the strength of fly ash-modified MPC mortar (FA-MPC) with curing time is illustrated in Fig. 4. It could be seen from Fig. 4 that the strength of FA-MPC increases with curing time increased, and the growth rates of the strength of FA-MPC with different incorporations were relatively consistent after 7 days of air-curing. Among them, 10% FA-MPC had higher strength than other FA-MPC with the same incorporation under the same conditions during the curing time studied and had a compressive strength increase of 11.6 MPa to rank first, but its increase of flexural strength was 1.6 MPa, which was only higher than 15% FA-MPC. It is known that after adding fly ash, the early strength of modified MPC mortar slightly decreased, but the later strength decreased significantly, the addition of 10% FA has a significant impact on the early flexural strength of MPC mortar, but has little effect on the later flexural strength. After FA is added more, the strength of modified MPC mortar decreased significantly. With the increase of fly ash content, more phosphates are adsorbed in MPC mortar, and less $MgKPO_4 \cdot 6H_2O$ is generated during hydration, making the system porous and reducing the compressive strength of MPC mortar.

The relationship between the strength of silica fume-modified MPC mortar (SF-MPC) and the curing time in Fig. 5 is almost the same as that of fly ash-modified MPC mortar. 15% SF-MPC had higher strength than other incorporation under the same conditions throughout the curing time studied, and also outperformed other SF-MPC with a compressive strength increase of 24.4 MPa, and ranked first with 10% SF-MPC with a flexural strength increase of 2.5 MPa. At the same curing age, when the SF content is less than 15%, the compressive

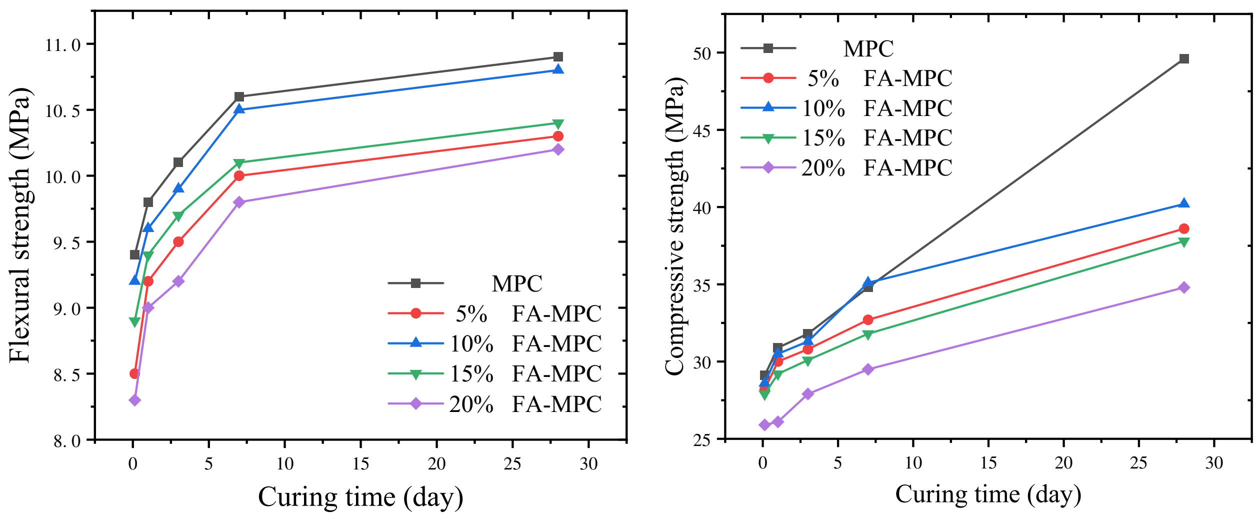

(a) Flexural strength **(b) Compressive strength**

Fig. 4 Strength change of FA-MPC

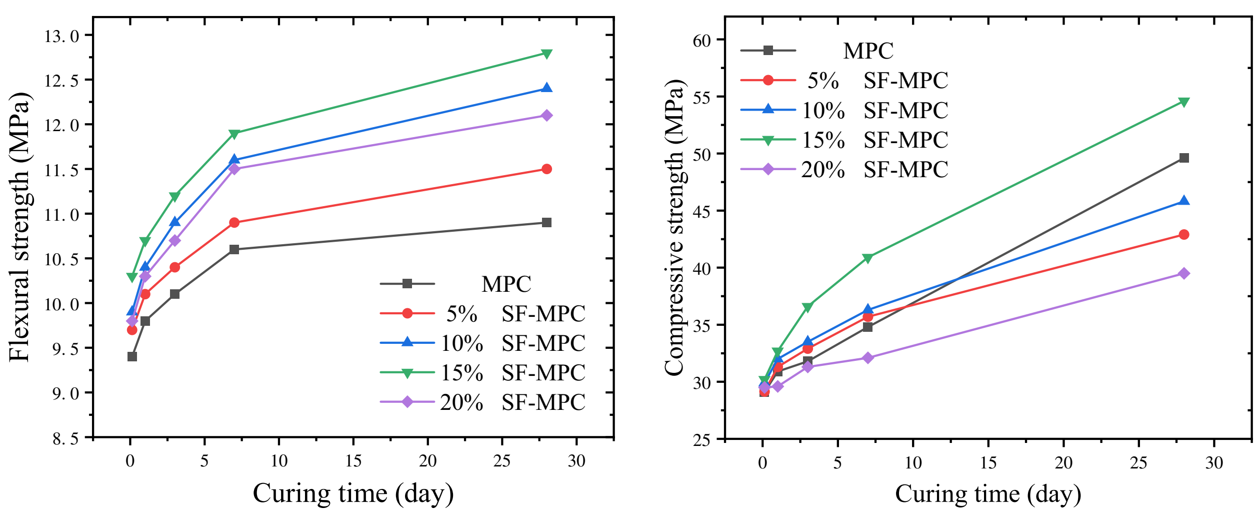

(a) Flexural strength **(b) Compressive strength**

Fig. 5 Strength change of SF-MPC

strength of MPC mortar increases with the increase of the content; when the content of SF exceeds 15%, the compressive strength of MPC mortar decreases. The reason may be that the reaction heat released by magnesium oxide and phosphate during the acid–base reaction can stimulate the silica component in the silica fume, and a small portion of amorphous SiO_2 and MgO react to form $MgSiO_3$, thereby improving the compactness of MPC mortar and promoting the strength of cement. However, excessive silica fume can weaken this strengthening effect, possibly because when the amount of silica fume is too large, the reaction heat released by acid–base reaction is absorbed by silica fume, but the heat is not enough to stimulate the subsequent reaction of silica fume, resulting in a decrease in compressive strength.

The relationship between strength and curing time of metakaolin-modified MPC mortar (MK-MPC) in Fig. 6 is also basically the same as that of fly ash-modified MPC mortar. The strength growth rate of 10% MK-MPC was significantly higher than that of other MK-MPC in each curing stage. At the same time, the strength of 10% MK-MPC was higher than that of other MK-MPC under

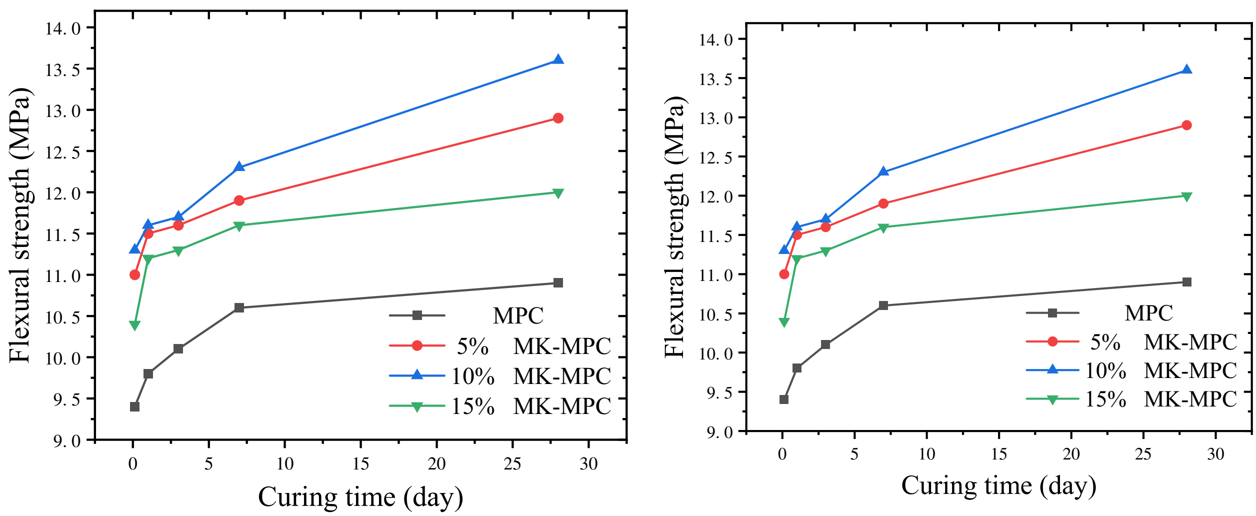

(a) Flexural strength (b) Compressive strength

Fig. 6 Strength change of MK-MPC

the same conditions in the whole studied curing time. And 10% MK-MPC had an increase in flexural strength of 2.3 MPa and compressive strength of 12.3 MPa to show the best performance among the three incorporations. When the content of metakaolin increases from 5 to 10%, the compressive strength of MPC mortar increases; When the incorporation increases from 10 to 15%, the compressive strength of modified MPC mortar decreases. The reason for this phenomenon may be that the addition of metakaolin reduces the main hydration products generated, thereby reducing the compressive strength of MPC mortar.

The strengths of the different minerals-modified MPC mortars in their optimum incorporations are compared in Fig. 7, to show the strength change with curing time. It could be found that the minerals that performed best in improving the flexural and compressive strength of the modified MPC mortars were not only. Metakaolin showed a significant flexural strength advantage during the studied curing time but was inferior to silica fume in terms of compressive strength. At the same time, after

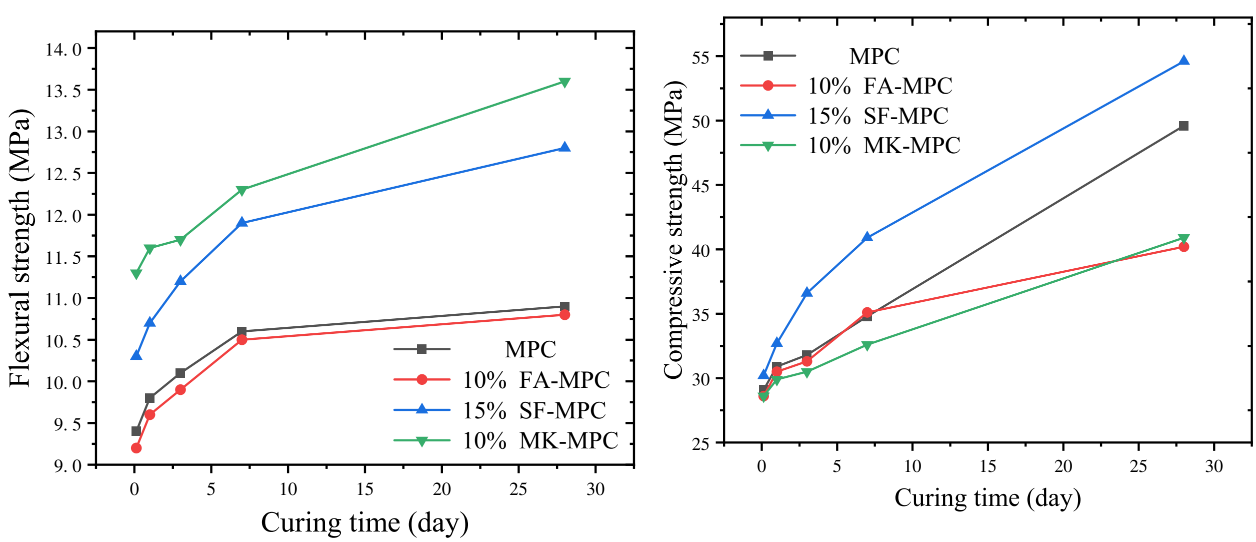

(a) Flexural strength (b) Compressive strength

Fig. 7 Strength change of different mineral admixtures modified MPC mortar in best incorporation

7 days of curing, metakaolin showed the highest strength growth rate, and at 28 days the compressive strength exceeded that of fly ash. It could be seen that different incorporations of the three minerals have different effects on the strength of modified MPC mortar and its development, so it is necessary to further elaborate and quantify the relationship between the incorporations & curing time of each mineral and the strength of modified MPC mortar for the application of modified MPC mortar.

3 Modified MPC Mortar Strength Calculation Model

3.1 Mathematical Analysis Model

Since the experimental design focused on the effect of mineral on strength development, only the effect of the two independent variables, curing time and mineral incorporations, on strength was considered. Mathematical models were used to obtain the relationships between the dependent variables (flexural strength (σ_f/MPa) and compressive strength (σ_c/MPa)) and the independent variables (mineral incorporations (I/%), and curing time (t/day)), to further quantify and analyze the relationship between mineral incorporations & curing time and MPC mortar strengths and compare the degree of influence of different minerals on MPC mortar strengths. Linear model, general nonlinear, and data distribution-shaped nonlinear model were chosen to describe the relationship between the independent and dependent variables.

3.1.1 Linear Model (LM)

A linear model is a simple tool for analyzing data and making analytical predictions. For linear models, the relationship between the independent and dependent variables is considered to be a simple linear relationship, i.e., the mineral incorporations and curing time are independent of each other and do not affect each other, and act directly on the strengths with their respective coefficients. Using a linear model, a simple relationship between the dependent and independent variables can be obtained quickly. In this study, the modeling analysis of modified MPC mortar strength data would be achieved utilizing the multiple-linear regression by establishing a binary linear model Eqs. (3), (4):

$$\sigma_f = \alpha_1 + \alpha_2 \times I + \alpha_3 \times t, \tag{3}$$

$$\sigma_c = \alpha_4 + \alpha_5 \times I + \alpha_6 \times t, \tag{4}$$

where $\alpha 1$, $\alpha 2$, $\alpha 3$ are the flexural strength model parameters and $\alpha 4$, $\alpha 5$, $\alpha 6$ are the compressive strength model parameters.

3.1.2 General Nonlinear Model (GNM)

A nonlinear model is a nonlinear combination function containing the model parameters by modeling the measured data. Unlike traditional linear models, a nonlinear model allows estimating models with arbitrary relationships between the independent and dependent variables. For nonlinear models, the interaction between independent variables is taken into account, i.e., the mineral incorporations and curing time are considered to be not independent of each other and influence each other to act on the dependent variable, but in order to get a more accurate fit for each data point, nonlinear models not only take more time, but also tend to lead to anomalous distributions in the solved model. Other strength models (Mohammed et al., 2020; Vipulanandan & Mohammed, 2018) were referred to set up a general nonlinear model (Yasar et al., 2012) Eqs. (5), (6) to model and analyze the modified MPC mortar strength data:

$$\sigma_f = \beta_1 \times I^{\beta_2} \times t^{\beta_3}, \tag{5}$$

$$\sigma_f = \beta_1 \times I^{\beta_2} \times t^{\beta_3}, \tag{6}$$

where β_1, β_2, β_3 are the flexural strength model parameters and β_4, β_5, β_6 are the compressive strength model parameters.

3.1.3 Data Distribution-Shaped Nonlinear Model (DDSNM)

The chosen model form often affects the fitting effect and leads to a situation of data overfitting in the process of performing model fitting. It means that random fluctuations in the data and experimental errors are also considered to be the actual composition of the relationship between variables (Hawkins, 2004), thus making it difficult to reflect the changing relationship between variables. To solve the possible overfitting problem of general nonlinear models, the distribution of samples' data points in space was interpolated by cubic polynomial interpolation (Hu, et al., 2008) and fitted surfaces were plotted (Figs. 8, 9, 10, 11, 12, 13). And then the characteristics of the surfaces were observed, and it was found that the distributions of MPC mortars modified with three different mineral materials in the variable space share the same characteristics. It was found that both in terms of flexural and compressive strengths, with constant mineral incorporation, the variation of strength with curing time was adapted to a logarithmic function, and in the case of a constant curing time, the variation of strength with mineral incorporations presented a curve with a wave peak.

Based on the above characteristics, the variation of modified MPC mortar strength with mineral incorporation (I) can be considered to be expressed in the form of a quadratic function and multiplied with time (t) to

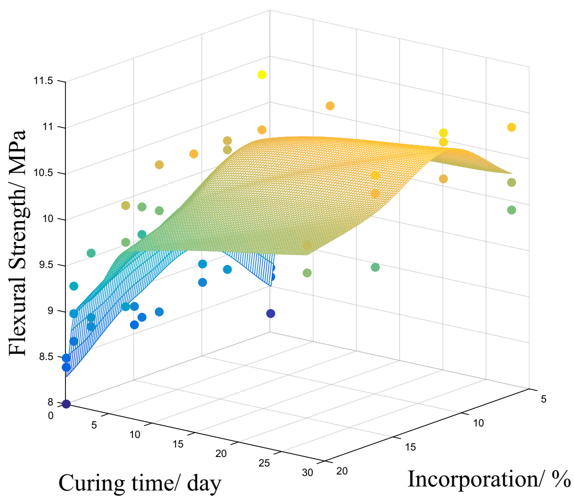

Fig. 8 Flexural strength distribution of FA-MPC

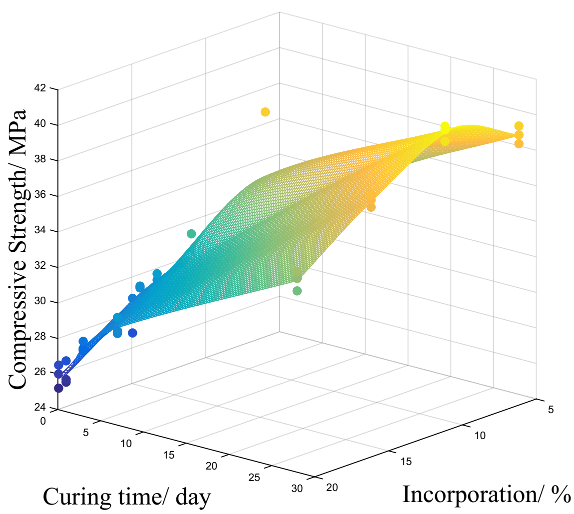

Fig. 9 Compressive strength distribution of FA-MPC

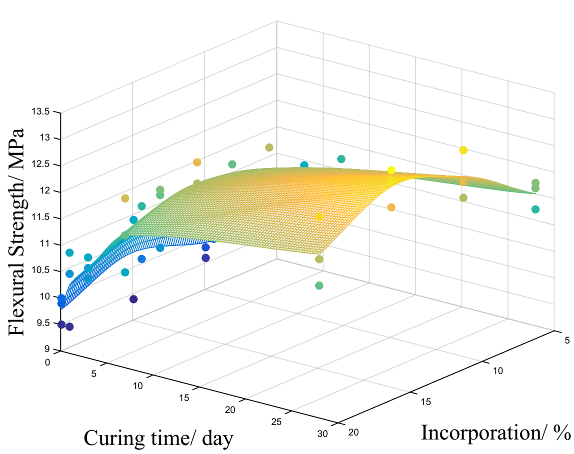

Fig. 10 Flexural strength distribution of SF-MPC

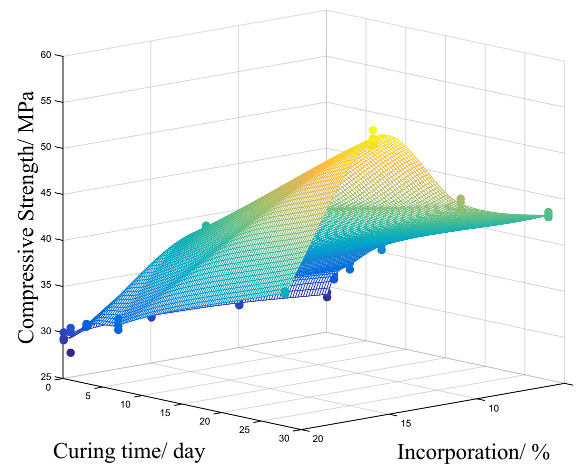

Fig. 11 Compressive strength distribution of SF-MPC

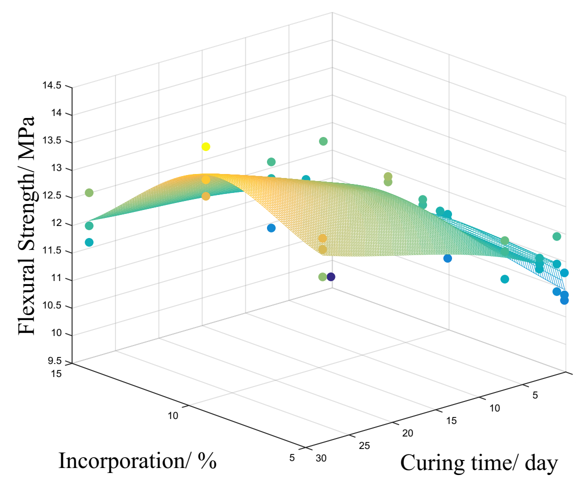

Fig. 12 Flexural strength distribution of MK-MPC

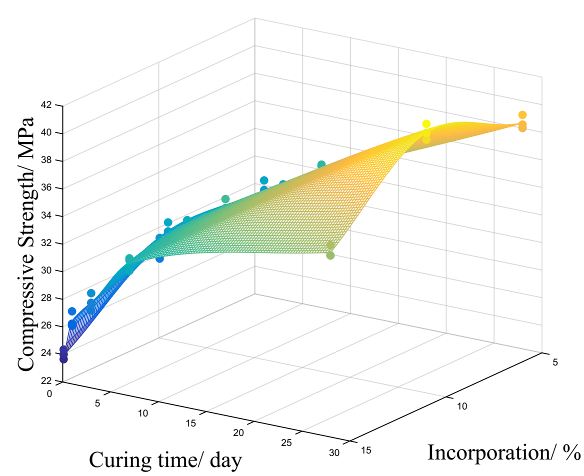

Fig. 13 Compressive strength distribution of MK-MPC

represent the interaction between time and mineral content. And the natural logarithmic function was chosen to represent the relationship between curing time and strength. Thus, the DDSNM of Eqs. (7), (8) were established to model the strength data for analysis:

$$\sigma_f = \gamma_1 + t \times \left(\gamma_2 \times I^2 + \gamma_3 \times I + \gamma_4\right) + \gamma_5 \times \ln t, \tag{7}$$

$$\sigma_c = \gamma_6 + t \times \left(\gamma_7 \times I^2 + \gamma_8 \times I + \gamma_9\right) + \gamma_{10} \times \ln t, \tag{8}$$

where γ_1, γ_2, γ_3, γ_4, γ_5 are the flexural strength model parameters and γ_6, γ_7, γ_8, γ_9, γ_{10} are the compressive strength model parameters.

All data measured in the test (FA:60 sets, SF:60 sets, MK:45 sets) would be used for regression calculations of the parameters in the proposed three mathematical models, and the mean value of every three replicate test samples was used as the test set to evaluate the model performance. R^2 and root mean square error (RMSE) would be selected to evaluate the model performance in combination with the reflection of the functional relationship on the spatial variation of the sample points. The R^2 indicates the proportion of the selected independent variable to explain the dependent variable's data fluctuation. The closer the R^2 approach to 1, the more tested data distributed close around the model and the more reasonably can the proposed model represent the dependent variable's data variation. The RMSE would be used to measure the deviation between the predicted value and the true value. It can reflect the prediction accuracy of the model at the observation points. The smaller the RMSE is, the more effective the model is.

3.2 FA-MPC Strength Model

The parameters in the binary linear model Eqs. (3) and (4) were calculated by using the "Linear" module of the "Regression" option in the "Analysis" menu of IBM SPSS Statistics 24 (IBM SPSS, 2013). According to Table 4, for the strength linear model (Strength-LM) of FA-MPC, the incorporations did not significantly affect the flexural strength, but it still negatively affected the flexural strength with a weight of 0.018, and the curing time significantly affected the flexural strength positively with a weight of 0.047. In terms of compressive strength, the incorporation significantly affected the compressive strength negatively with a weight of 0.229, and the curing time significantly affected the compressive strength positively with a weight of 0.338.

According to the regression coefficients, the spatial distribution of the Strength-LM space mesh is plotted to reflect the development of the strength of the modified MPC mortar with different fly ash incorporations over time and the spatial distribution of the test set is also plotted (Fig. 14a, c). It is found that although the test set data are mostly distributed near the Strength-LM space mesh, the model does not well reflect the distribution and change of the data. The error performance of the model is shown in Fig. 14b, d. The calculation error of the flexural strength calculation model for the test set is between − 10% and 12.5%, and the error of the compressive strength calculation model is between − 10% and 10%. The error of Strength-LM in predicting the strength of FA-MPC mortar does not exceed 12.5%. The R^2 of the models are 0.420 and 0.861, which indicates that Strength-LM including the mineral incorporation and curing time can explain 42.0% and 86.1% of the fluctuation of flexural strength and compressive strength data.

The Sequential Quadratic Programming (SQP) algorithm (Gill & Wong, 2012) was selected using the "Nonlinear" module of the "Regression" option in the "Analysis" menu of IBM SPSS Statistic with a 95% confidence level. The parameters in the strength general nonlinear model (Strength-GNM) Eqs. (5), (6) were calculated by iterative regression. According to Table 5, for the GNM of fly ash-modified MPC mortar strength, the software obtained the minimum residual sum of squares (RSS) and the optimal estimated parameters for the flexural strength calculation model and the compressive strength calculation model by 24 and 26 iterations.

According to the regression coefficients, the spatial distribution of the Strength-GNM space mesh is plotted to reflect the development of the strength of the FA-MPC

Table 4 Regression coefficient of LM (FA-MPC)

Model type	α_1	α_2	*P*-value	α_3	*P*-value	Durbin–Watson	VIF
Flexural strength	9.484	− 0.018	0.197	0.047	0.000	1.633	1
Model type	α_4	α_5	*p*-value	α_6	*P*-value	Durbin–Watson	VIF
Compressive strength	31.563	− 0.229	0.000	0.338	0.000	0.974	1

P-Value is the significant index of the calculated regression coefficient, which is significant if it is less than 0.05; Durbin Watson is used to test the independence between samples, and the closer its value to 2, the stronger the independence between samples, and the higher the reliability of the calculation results. VIF is the Variance Inflation Factor, the closer its value is to 1, the lighter the degree of multicollinearity between independent variables, and on the contrary, the heavier.

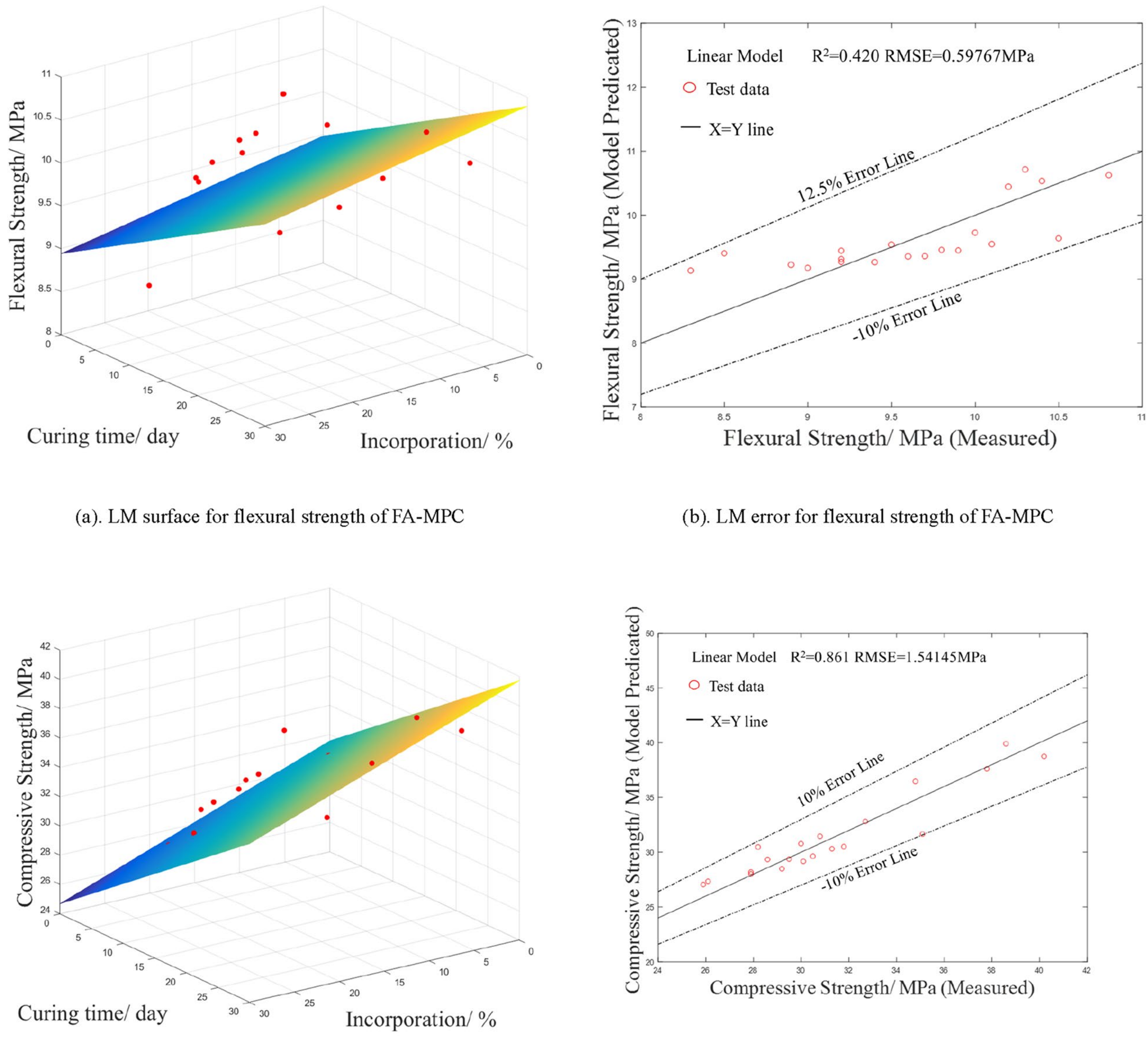

(a). LM surface for flexural strength of FA-MPC

(b). LM error for flexural strength of FA-MPC

(c). LM surface for compressive strength of FA-MPC

(d). LM surface for compressive strength of FA-MPC

Fig. 14 Strength-LM performance of FA-MPC

with different incorporations over time, and the spatial distribution of the test set is also plotted (Fig. 15a, c). It is found that the test set data are mostly distributed near the Strength-GNM space mesh, and the model could well reflect the distribution and change of the data. However, it is not a reasonable description of the strength change with incorporations in 28d air cured. The error performance of the model is shown in Fig. 15b, d. The calculation error of the flexural strength calculation model for the test set is between − 5% and 5%, and the error of the compressive strength calculation model is between − 10% and 10%. The error of Strength-GNM in predicting the strength of FA-MPC mortar does not exceed 10%. The R^2 of the models are 0.604 and 0.752, which indicates that Strength-GNM including the mineral incorporation

Table 5 Regression coefficient of GNM (FA-MPC)

Model type	Iteration	RSS	β_1	β_2	β_3
Flexural strength	24	13.911	9.561	− 0.010	0.034
Model type	Iteration	RSS	β_4	β_5	β_6
Compressive strength	26	240.871	34.442	− 0.064	0.060

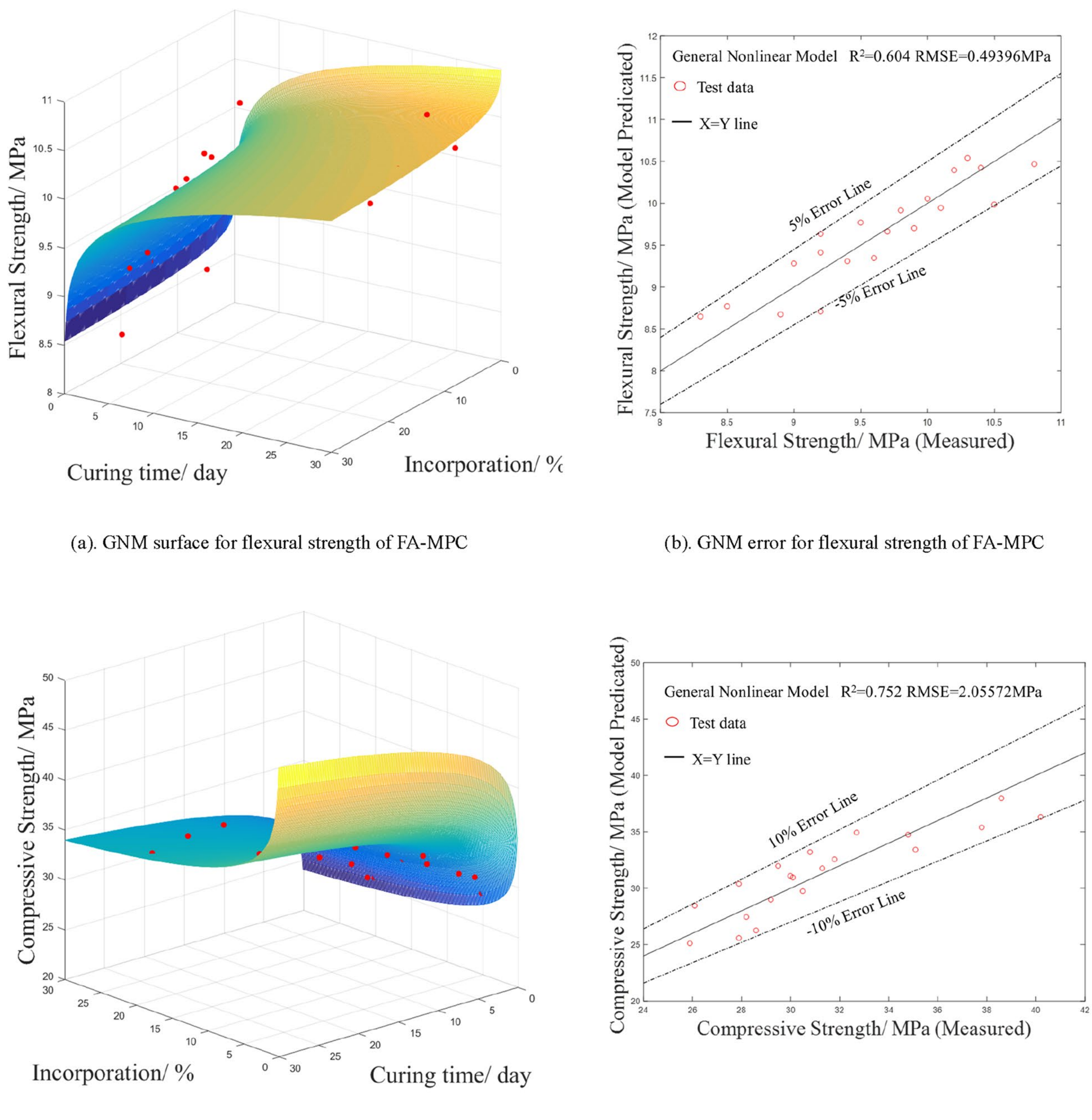

(a). GNM surface for flexural strength of FA-MPC

(b). GNM error for flexural strength of FA-MPC

(c). GNM surface for compressive strength of FA-MPC

(d). GNM error for compressive strength of FA-MPC

Fig. 15 Strength-GNM performance of FA-MPC

and curing time can explain 60.4% and 75.2% of the fluctuation of flexural strength and compressive strength data.

The curve fitting application package in Matlab 2016b (MathWorks, 2016b) was used to perform regression calculations for the parameters in the strength data distribution-shaped nonlinear model (Strength-DDSNM) Eqs. (7), (8). As shown in Table 6, the sum of squares of error (SSE) for the flexural strength model and compressive strength model are 13.2 and 127.9, which are both smaller than the SSE in the general nonlinear model.

According to the regression coefficients, the spatial distribution of the Strength-DDSNM space mesh is plotted to reflect the development of the strength of the FA-MPC with different incorporations over time, and the spatial distribution of the test set is also plotted (Fig. 16 a, c). It

Table 6 Regression coefficient of DDSNM (FA-MPC)

Model type	γ_1	γ_2	γ_3	γ_4	γ_5	SSE
Flexural strength	9.338	-3.424×10^{-4}	7.828×10^{-3}	-3.119×10^{-2}	0.3119	13.2
Model type	γ_6	γ_7	γ_8	γ_9	γ_{10}	SSE
Compressive strength	28.27	-20.6×10^{-4}	39.17×10^{-3}	14.14×10^{-2}	0.6591	127.9

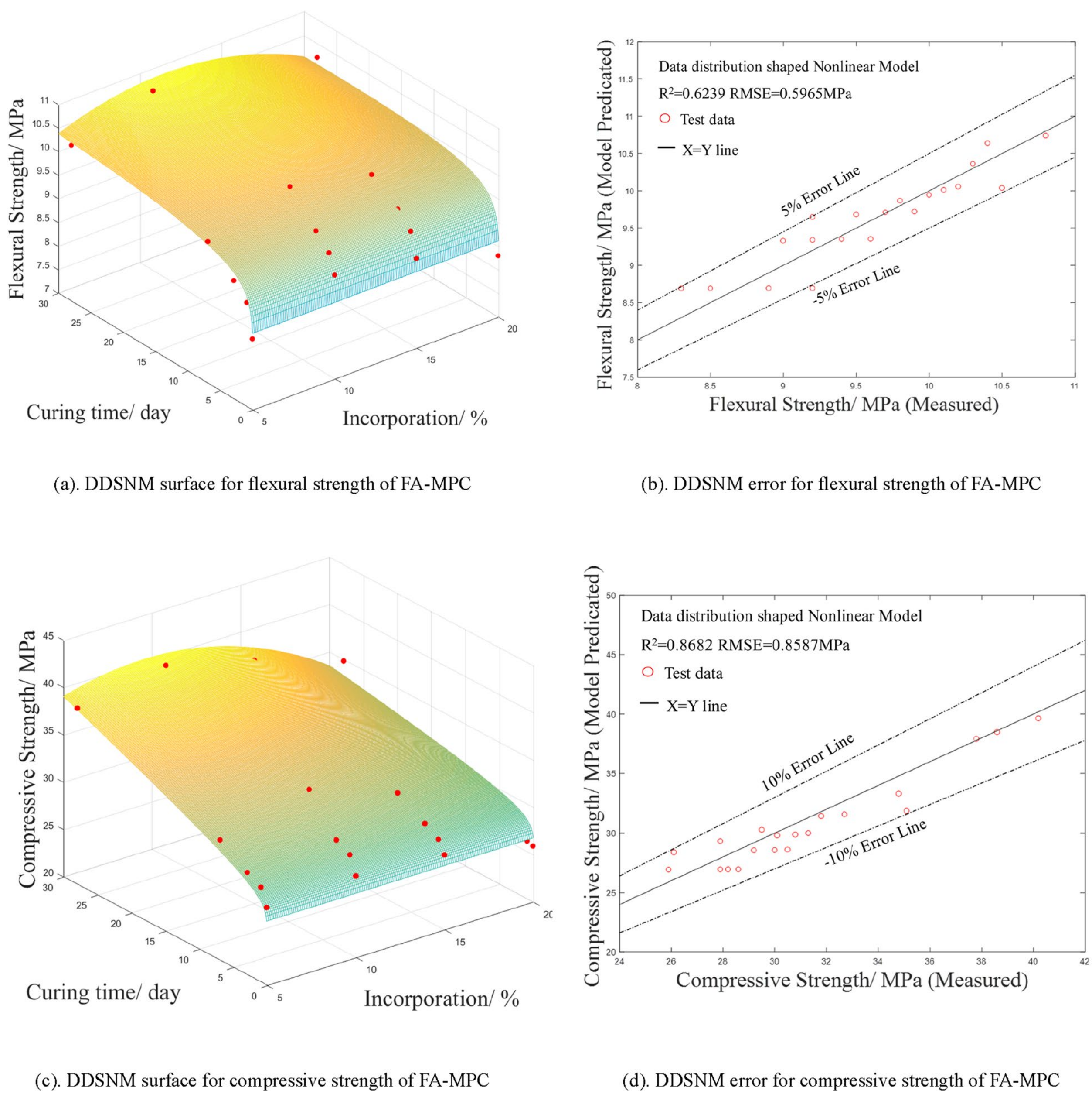

Fig. 16 Strength-DDSNM performance of FA-MPC

is found that the test set data are mostly distributed near the Strength-DDSNM space mesh, and the model could well reflect the distribution and change of the data. The error performance of the model is shown in Fig. 16b, d. The calculation error of the flexural strength calculation model for the test set is between − 5% and 5%, and the error of the compressive strength calculation model is between − 10% and 10%. The error of Strength-DDSNM in predicting the strength of FA-MPC mortar does not exceed 10%. The R^2 of the models are 0.6239 and 0.8682, which indicates that Strength-DDSNM including the mineral incorporation and curing time can explain 62.39% and 86.82% of the fluctuation of flexural strength and compressive strength data.

3.3 SF-MPC Strength Model

As with the calculation of the three model parameters in Sect. 3.2, only the calculation results would be shown and analyzed in the following part. According to Table 7, for the strength linear model (Strength-LM) of SF-MPC, the incorporations significantly affected the flexural strength positively with a weight of 0.069, but the curing time did not significantly affect the flexural strength, while with a positive trend in weight of 0.047. Although the incorporation did not significantly affect the compressive strength, it still negatively affected the compressive strength with a weight of 0.0049. And the curing time significantly affected the compressive strength positively with a weight of 0.535.

According to the regression coefficients, the spatial distribution of the Strength-LM space mesh is plotted to reflect the development of the strength of the SF-MPC with different incorporations over time and the spatial distribution of the test set is also plotted (Fig. 17. a, c). It is found that although the test set data are mostly distributed near the Strength-LM space mesh and the growth trend of the data can be well described, the model does not well reflect the characteristic of the data fluctuation. The error performance of the model is shown in Fig. 17. b, d. The calculation error of the flexural strength calculation model for the test set is between − 7.5% and 10%, and the error of the compressive strength calculation model is between − 15% and 15%. The error of Strength-LM in predicting the strength of SF-MPC mortar does not exceed 15%. The R^2 of the models are 0.589 and 0.747, which indicates that Strength-LM including the mineral incorporation and curing time can explain 58.9% and 74.7% of the fluctuation of flexural strength and compressive strength data.

According to Table 8, for the GNM of SF-MPC strength, the software obtained the RSS and the optimal estimated parameters for the flexural strength calculation model and the compressive strength calculation model by 23 and 27 iterations.

According to the regression coefficients, the spatial distribution of the Strength-GNM space mesh is plotted to reflect the development of the strength of the SF-MPC with different incorporations over time, and the spatial distribution of the test set is also plotted (Fig. 18a, c). It is found that the test set data are mostly distributed near the Strength-GNM space mesh, and the model could well reflect the distribution and change of the data in a short curing time. However, it cannot precisely describe the strength change with incorporations in 28d air cured. The error performance of the model is shown in Fig. 18b, d. The calculation error of the flexural strength calculation model for the test set is between − 5% and 5%, and the error of the compressive strength calculation model is between − 12.5% and 18.75%. The error of Strength-GNM in predicting the strength of SF-MPC mortar does not exceed 18.75%. The R^2 of the models are 0.715 and 0.661, which indicates that Strength-GNM including the mineral incorporation and curing time can explain 71.5% and 66.1% of the fluctuation of flexural strength and compressive strength data.

Table 9 shows the calculated results of parameters in Eqs. (7), (8) of the Strength-DDSNM of SF-MPC, it can be seen that the SSE of the flexural strength model and compressive strength model are 13.46 and 259.1, which are smaller than the SSE in the GNM.

According to the regression coefficients, the spatial distribution of the Strength-DDSNM space mesh is plotted to reflect the development of the strength of the SF-MPC with different incorporations over time, and the spatial distribution of the test set is also plotted (Fig. 19. a, c). It is found that the test set data are mostly distributed near the Strength-DDSNM space mesh, and the model could well reflect the distribution and change of the data. The error performance of the model is shown in Fig. 19b, d. The calculation error of

Table 7 Regression coefficient of LM (SF)

Model type	α_1	α_2	*P*-value	α_3	*P*-value	Durbin–Watson	VIF
Flexural strength	10.057	0.069	0.000	0.029	0.055	1.594	1
Model type	α_4	α_5	*P*-value	α_6	*P*-value	Durbin–Watson	VIF
Compressive strength	31.754	− 0.049	0.521	0.535	0.000	0.375	1

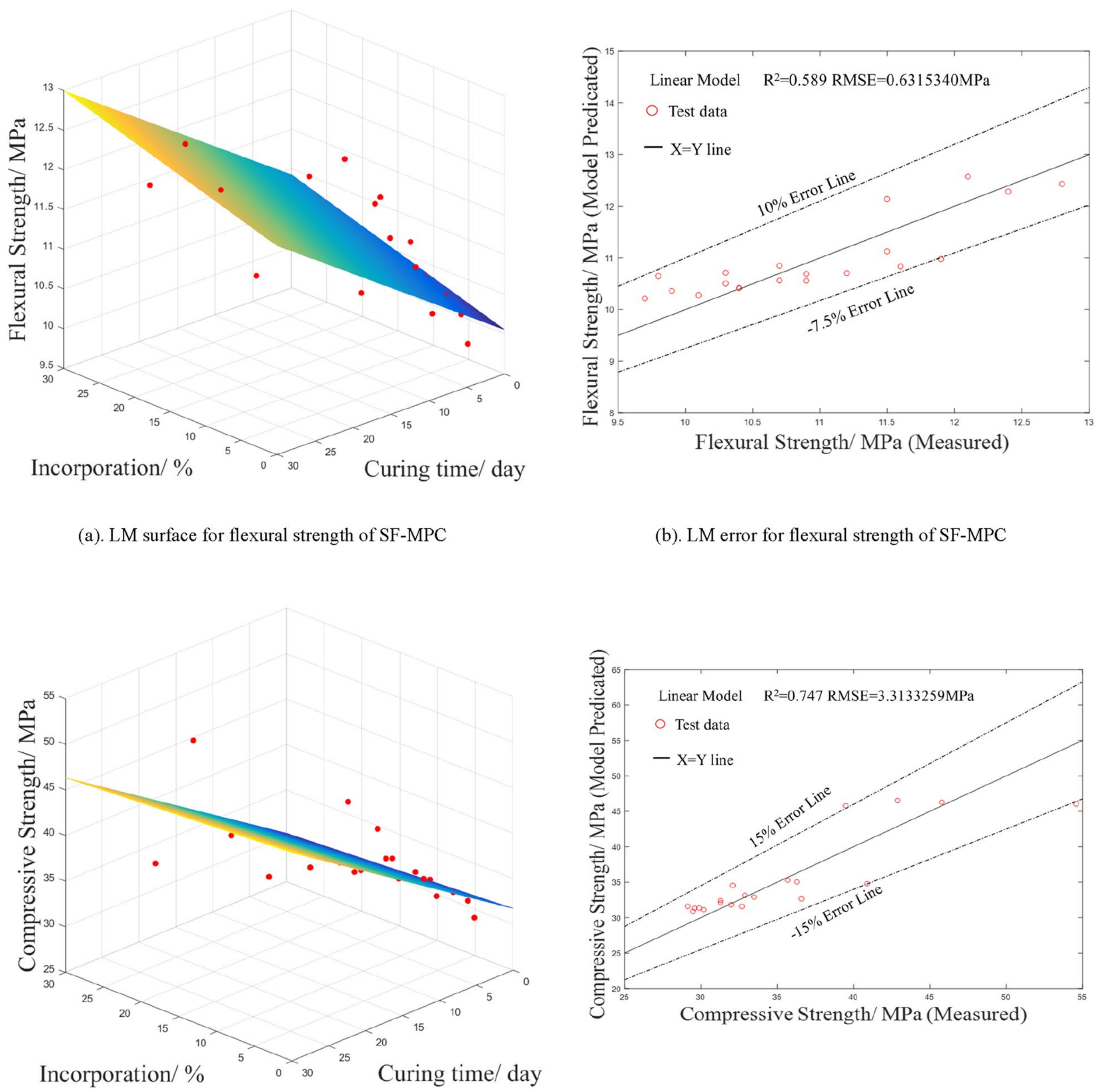

(a). LM surface for flexural strength of SF-MPC

(b). LM error for flexural strength of SF-MPC

(c). LM surface for compressive strength of SF-MPC

(d). LM error for compressive strength of SF-MPC

Fig. 17 Strength-LM performance of SF-MPC

Table 8 Regression coefficient of GNM (SF)

Model type	Iteration	RSS	β_1	β_2	β_3
Flexural strength	23	15.758	9.678	0.036	0.040
Model type	Iteration	RSS	β_4	β_5	β_6
Compressive strength	27	839.490	32.122	0.004	0.086

the flexural strength calculation model for the test set is between − 5% and 5%, and the error of the compressive strength calculation model is between − 10% and 12.5%. The error of Strength-DDSNM in predicting the strength of SF-MPC mortar does not exceed 12.5%. The R^2 of the models are 0.7566 and 0.8953, which indicates that Strength-DDSNM including the mineral incorporation and curing time can explain 75.66% and 89.53%

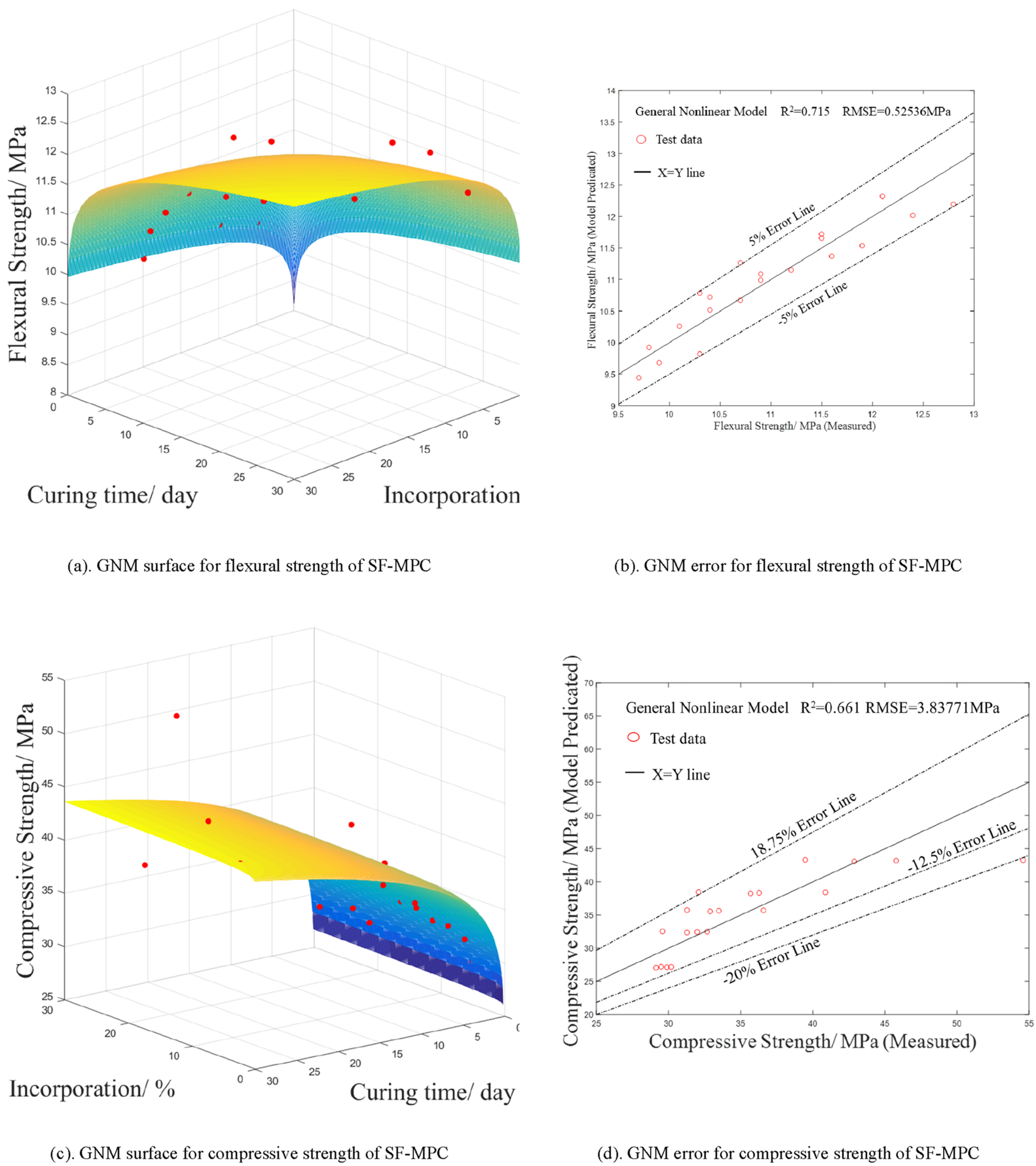

(a). GNM surface for flexural strength of SF-MPC

(b). GNM error for flexural strength of SF-MPC

(c). GNM surface for compressive strength of SF-MPC

(d). GNM error for compressive strength of SF-MPC

Fig. 18 Strength-GNM performance of SF-MPC

of the fluctuation of flexural strength and compressive strength data.

3.4 MK-MPC Strength Model

According to Tables 10, 11 for Strength-LM of MK-MPC, the incorporations significantly affected the flexural strength negatively with a weight of 0.048, and the curing time significantly affected the flexural strength positively with a weight of 0.059. In terms of compressive strength, the incorporation significantly affected the compressive strength negatively with a weight of 0.254, and the curing

Table 9 Regression coefficient of DDSNM (SF)

Model type	γ_1	γ_2	γ_3	γ_4	γ_5	SSE
Flexural strength	10.49	-6.681×10^{-4}	18.62×10^{-3}	-8.228×10^{-2}	0.3108	13.46
Model type	γ_6	γ_7	γ_8	γ_9	γ_{10}	SSE
Compressive strength	31.37	-70.16×10^{-4}	173.2×10^{-3}	-44.43×10^{-2}	0.9105	259.1

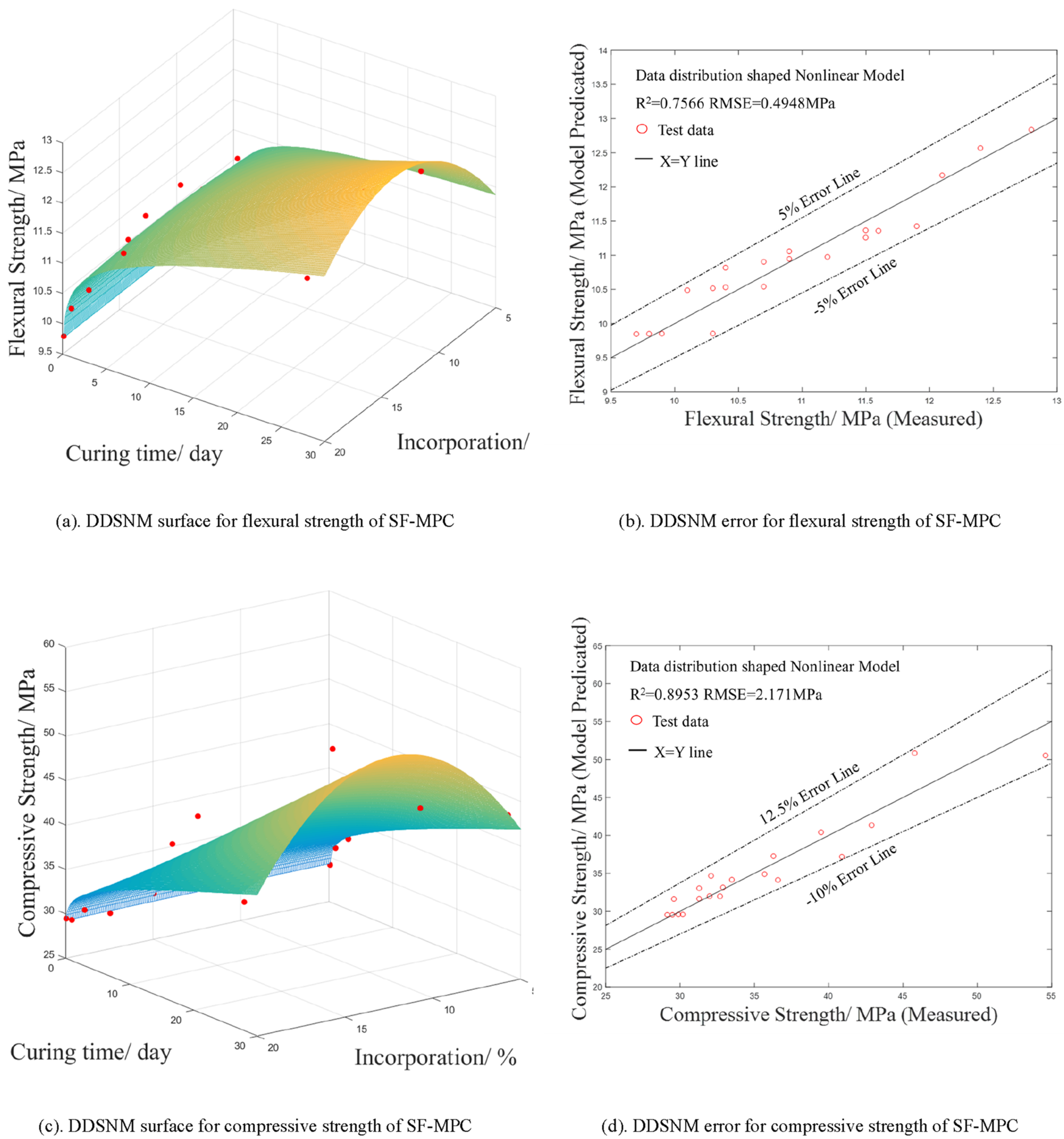

(a). DDSNM surface for flexural strength of SF-MPC

(b). DDSNM error for flexural strength of SF-MPC

(c). DDSNM surface for compressive strength of SF-MPC

(d). DDSNM error for compressive strength of SF-MPC

Fig. 19 Strength-DDSNM performance of SF-MPC

Table 10 Regression coefficient of LM (MK)

Model type	α_1	α_2	*P*-value	α_3	*P*-value	Durbin–Watson	VIF
Flexural strength	11.748	− 0.048	0.000	0.059	0.000	1.8	1
Model type	α_4	α_5	*P*-value	α_6	*P*-value	Durbin–Watson	VIF
Compressive strength	30.768	− 0.254	0.000	0.370	0.000	0.826	1

Table 11 Regression coefficient of GNM (MK)

Model type	Iteration	RSS	β_1	β_2	β_3
Flexural strength	23	13.952	12.162	− 0.029	0.029
Model type	Iteration	RSS	β_4	β_5	β_6
Compressive strength	28	192.039	33.085	− 0.057	.066

time significantly affected the compressive strength positively with a weight of 0.370.

According to the regression coefficients, the spatial distribution of the Strength-LM space mesh is plotted to reflect the development of the strength of the MK-MPC with different incorporations over time and the spatial distribution of the test set is also plotted (Fig. 20. a, c). It is found that the test set data are mostly distributed near the Strength-LM space mesh, and the model could fairly well reflect the increasing trend of the data, but the model does not do well in describing the distribution and change of the data. The error performance of the model is shown in Fig. 20b, d. The calculation error of the flexural strength calculation model for the test set is between − 5% and 6.25%, and the error of the compressive strength calculation model is between − 6.25% and 12.5%. The error of Strength-LM in predicting the strength of MK-MPC mortar does not exceed 12.5%. The R^2 of the models are 0.570 and 0.868, which indicates that Strength-LM including the mineral incorporation and curing time can explain 57.0% and 86.8% of the fluctuation of flexural strength and compressive strength data.

According to Table 11, for the GNM of SF-MPC strength, the software obtained the RSS and the optimal estimated parameters for the flexural strength calculation model and the compressive strength calculation model by 23 and 27 iterations.

According to the regression coefficients, the spatial distribution of the Strength-GNM space mesh is plotted to reflect the development of the strength of the MK-MPC with different incorporations over time, and the spatial distribution of the test set is also plotted (Fig. 21a, c). It is found that the deviation of the test data from the model is not too large during the short curing time, and the model could roughly reflect the variation of strength with incorporations, but with the growth of curing time, the deviation of the description of the variation of strength with incorporations becomes too large and unreasonable. The error performance of the model is shown in Fig. 21b, d. The calculation error of the flexural strength calculation model for the test set is between − 15% and 2.5%, and the error of the compressive strength calculation model is between − 6.25% and 25%. The error of Strength-GNM in predicting the strength of MK-MPC mortar does not exceed 25%. The R^2 of the models are 0.565 and 0.765, which indicates that Strength-GNM including the mineral incorporation and curing time can explain 56.5% and 76.5% of the fluctuation of flexural strength and compressive strength data.

Table 12 shows the calculated results of parameters in Eqs. (7), (8) of the Strength-DDSNM of MK-MPC mortar, it can be seen that the SSE of the flexural strength model and compressive strength model are 8.862 and 76.54, which are smaller than the SSE in the GNM.

According to the regression coefficients, the spatial distribution of the Strength-DDSNM space mesh is plotted to reflect the development of the strength of the MK-MPC with different incorporations over time, and the spatial distribution of the test set is also plotted (Fig. 22a, c). It is found that the test set data are mostly distributed near the Strength-DDSNM space mesh, and the model could well reflect the distribution and change of the data. The error performance of the model is shown in Fig. 22b, d. The calculation error of the flexural strength calculation model for the test set is between − 3.75% and 5%, and the error of the compressive strength calculation model is between − 5% and 11.25%. The error of Strength-DDSNM in predicting the strength of MK-MPC mortar does not exceed 11.25%. The R^2 of the models are 0.724 and 0.9062, which indicates that Strength-DDSNM including the mineral incorporation and curing time can explain 72.4% and 90.62% of the fluctuation of flexural strength and compressive strength data.

In general, with regard to the curing time and minerals incorporations, the form of Strength-DDSNM amply illustrates the evolution of the strength of mineral-modified MPC. When the curing period is determined, the strength tends to rise and then fall as the amount of incorporations increases, and the strength fluctuates more visibly with incorporations increased as the

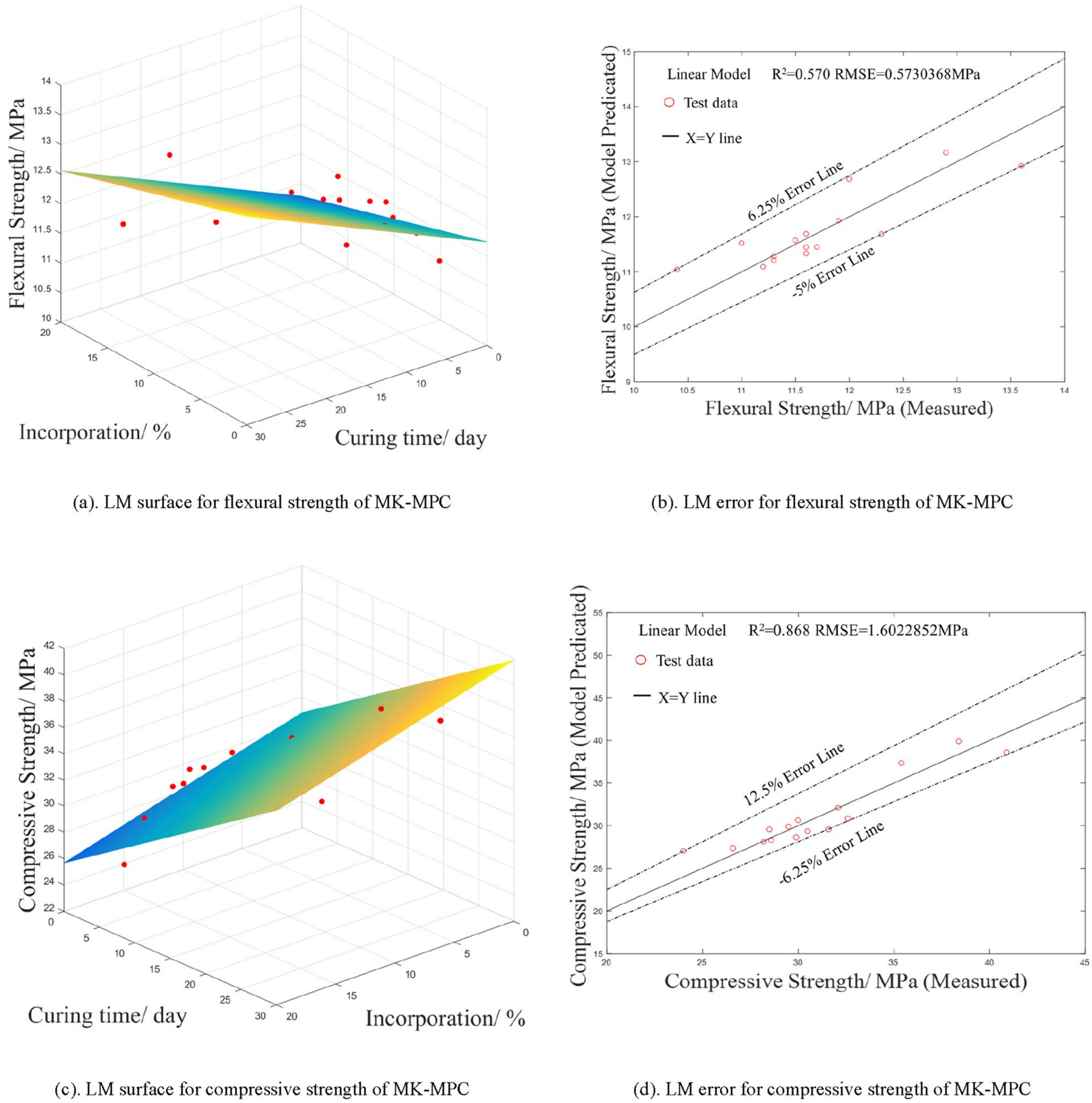

(a). LM surface for flexural strength of MK-MPC

(b). LM error for flexural strength of MK-MPC

(c). LM surface for compressive strength of MK-MPC

(d). LM error for compressive strength of MK-MPC

Fig. 20 Strength-LM performance of MK-MPC

curing time rises. When the incorporation is constant, the strength exhibits a feature of growing quickly at first, then slowing down as the curing time increases. On the other hand, when the incorporation is increased within a specific range, the strength grows more quickly per unit of time.

4 Evaluation of the Effect of the Different Minerals on Strength

In the previous analysis, DDSNM showed the best ability to describe the data distribution and development trend and also had the smallest errors and largest R^2, among the three models. To quantify the ability of different minerals to affect the strength in different incorporations and curing time, the strength influence coefficient is

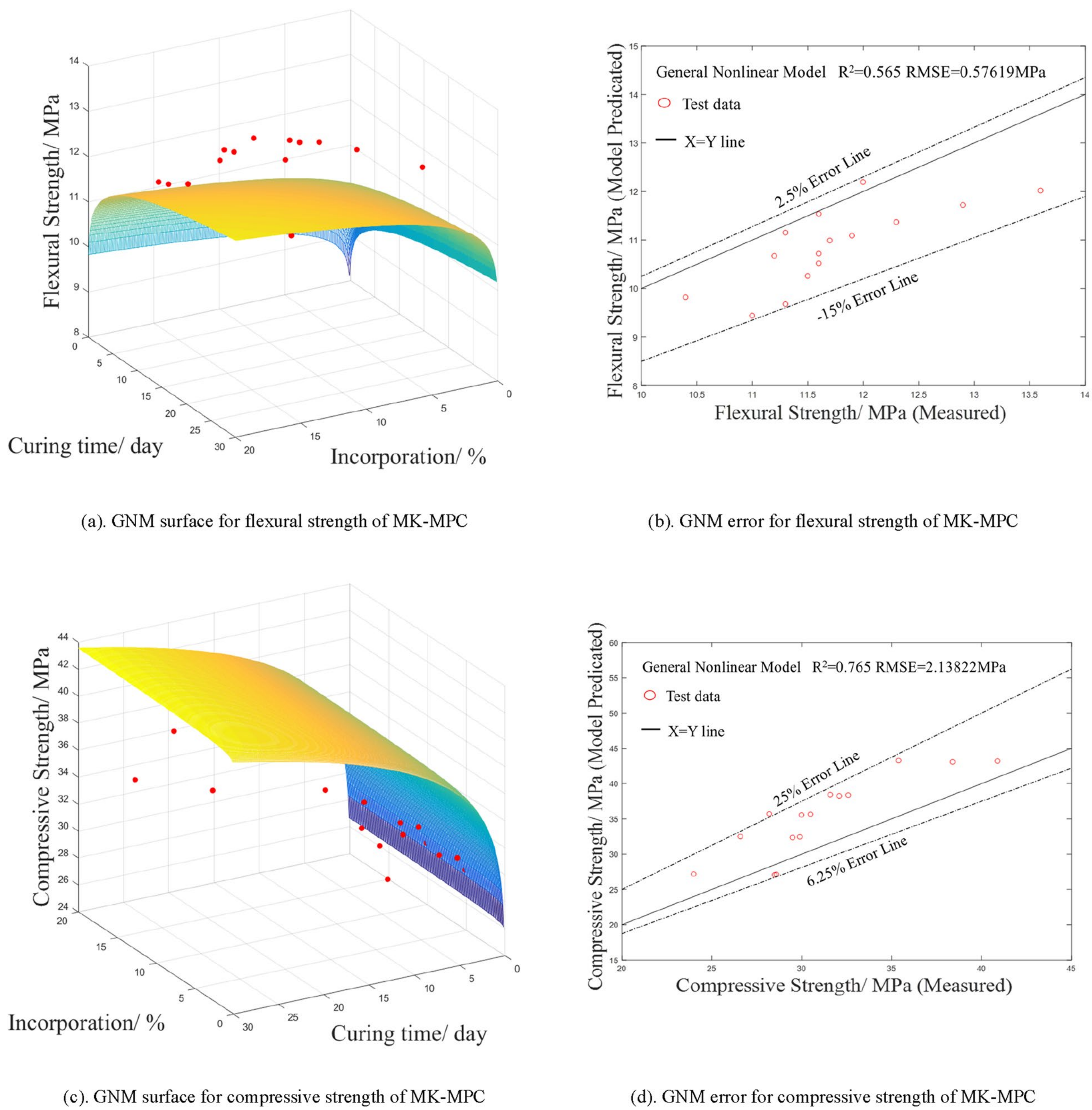

(a). GNM surface for flexural strength of MK-MPC

(b). GNM error for flexural strength of MK-MPC

(c). GNM surface for compressive strength of MK-MPC

(d). GNM error for compressive strength of MK-MPC

Fig. 21 Strength-GNM performance of MK-MPC.

Table 12 Regression coefficient of data distribution-shaped nonlinear model (SF)

Model type	γ_1	γ_2	γ_3	γ_4	γ_5	SSE
Flexural strength	11.32	-17.62×10^{-4}	31.84×10^{-3}	-8.15×10^{-2}	0.1913	8.862
Model type	γ_6	γ_7	γ_8	γ_9	γ_{10}	SSE
Compressive strength	28.41	-58.64×10^{-4}	105.9×10^{-3}	-10.63×10^{-2}	0.7134	76.54

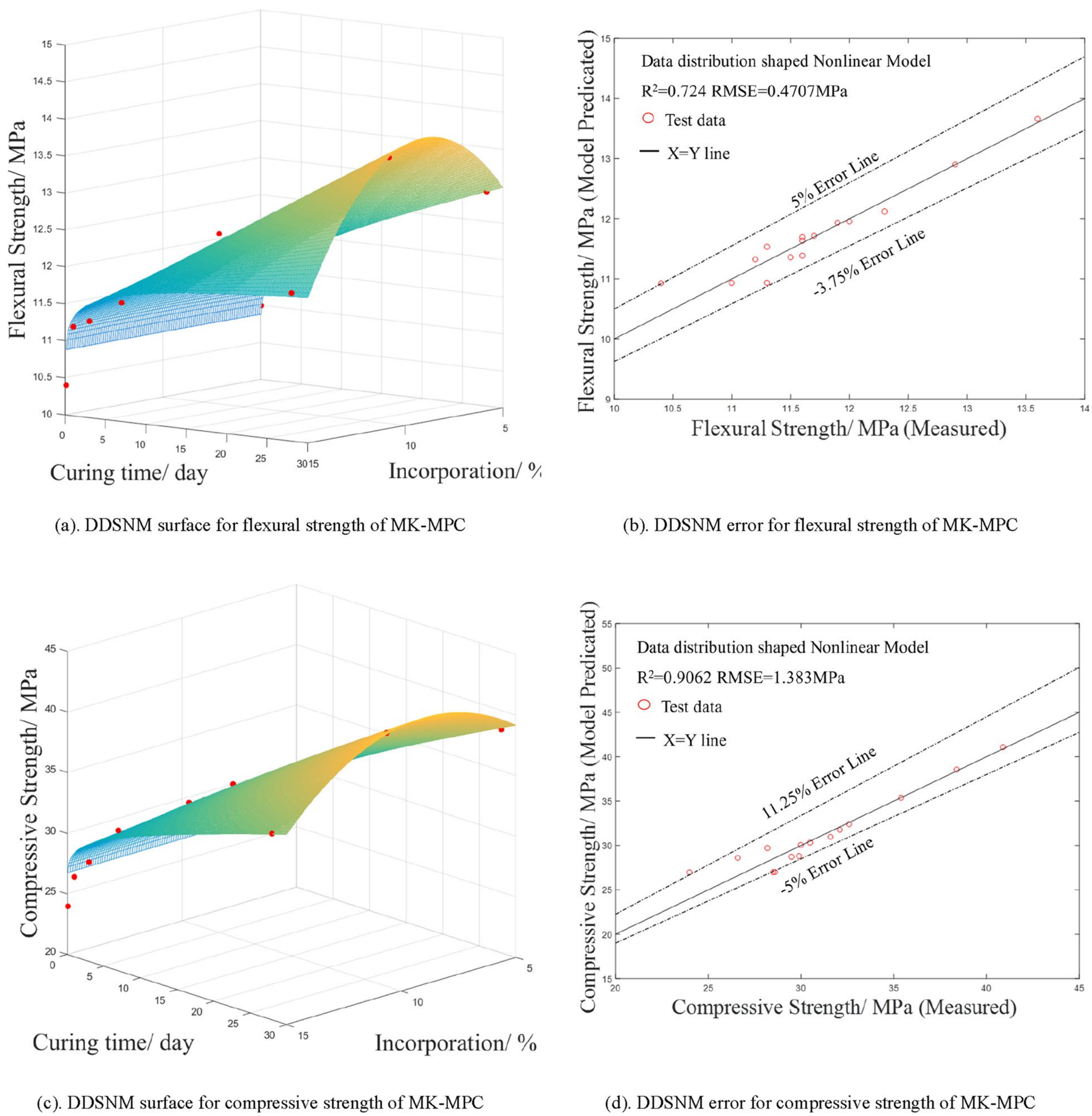

Fig. 22 Strength-DDSNM performance of MK-MPC

obtained by taking the partial derivative of the Strength-DDSNM Eqs. (7), (8) on the incorporation and curing time, respectively. By taking partial derivatives of the incorporation of the strength model, $d\sigma/dI$, the relationship between strength and mineral content variation, $F_{\sigma f,I}$ and $F_{\sigma c,I}$, could be obtained. Eqs. (9) and (11) express the mathematical relationship between the strength variation and the incorporation amount. It can be seen that curing time directly affects the growth of the strength in the incorporation amount, while the product relationship, $2\gamma \times t \times I$, shows that the change of curing time will amplify the influence of the incorporation amount on the strength variation rate. It was possible to determine the link between strength variation and curing time, $F_{\sigma f,t}$ and $F_{\sigma c,t}$, by calculating partial derivatives of the strength model's inclusion, $d\sigma/dt$. The mathematical relationship between the strength variation and the curing time is expressed by Eqs. (10) and (12). It is evident that incorporation influences the strength growth in the curing time, however the additive relationship in the equation indicates that the curing time has no major impact on the strength growth rate under the same incorporation.

It is also noted that when the curing time is small, the values of Eqs. (7) and (8) are approximately equal to γ_1 and γ_6, and then the strengths subsequently develop on the basis of γ_1 and γ_6, which can be regarded as the initial strength capacity coefficients. It can represent the initial strength of mineral-modified MPC mortar and reflect the influence of mineral materials on the initial strength:

$$f_{\sigma_f,I} = t \times (2\gamma_2 \times I + \gamma_3), \tag{9}$$

$$f_{\sigma_f,t} = \left(\gamma_2 \times I^2 + \gamma_3 \times I + \gamma_4\right) + \frac{\gamma_5}{t}, \tag{10}$$

$$f_{\sigma_c,I} = t \times (2\gamma_7 \times I + \gamma_9), \tag{11}$$

$$f_{\sigma_c,t} = \left(\gamma_7 \times I^2 + \gamma_8 \times I + \gamma_9\right) + \frac{\gamma_{10}}{t}. \tag{12}$$

The 28-day curing time (t = 28) and the optimum incorporation of the three mineral-modified MPC mortars are substituted into Eqs. (9), (10), (11), (12) to obtain the relevant performance parameters of the three mineral materials (Table 13). And XRD (Fig. 23) and SEM tests (Fig. 24) were conducted for 10% FA-MPC, 15% SF-MPC, and 10% MK-MPC under natural curing conditions.

According to Eqs. (9), (10), (11), (12) and the shape of DDSNM, the optimum content of the mineral for the maximum strength would appeared in the interval of the experiment incorporations and could be obtain by setting Eqs. (9), (10), (11), (12) = 0 and solving the equations. The optimum incorporation is expressed as Eqs. (13) and (14):

$$I_{op,\sigma_f} = -\frac{\gamma_3}{2\gamma_2}, \tag{13}$$

$$I_{op,\sigma_c} = -\frac{\gamma_9}{2\gamma_7}. \tag{14}$$

Table 13 Strength parameter of different mineral admixtures modified MPC mortar in best incorporation for 28d

Strength parameter	10% FA-MPC	15% SF-MPC	10% MK-MPC
γ_1	9.338	10.49	11.32
$f_{\sigma_{f,I}}$	0.0274	– 0.0398	– 0.0952
$f_{\sigma_{f,t}}$	0.0240	0.0578	0.0675
γ_6	28.27	31.37	28.41
$f_{\sigma_{c,I}}$	– 0.0568	– 1.0438	– 0.3186
$f_{\sigma_{c,t}}$	0.3506	0.6076	0.3918

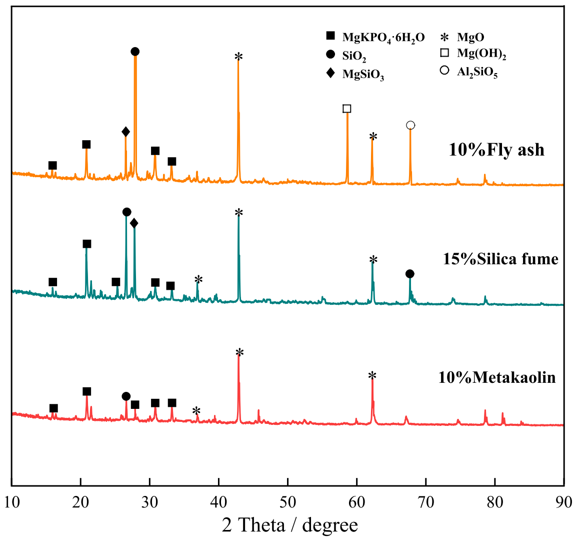

Fig. 23 XRD test results of modified MPC mortar after air-curing for 28 days

By substituting the DDSNM parameters of three mineral materials into Eqs. (13) and (14), the theoretical optimal incorporation can be calculated.

The characteristic peaks of the three modified MPC mortars are relatively the same in Fig. 23, which indicates that the hydration product $MgKPO_4$-$6H_2O$ (MKP) and unreacted MgO are both in the three modified MPC mortars. The hydration product MKP and MgO both provide the strength guarantee for the materials. MPC mortar forms a denser internal microstructure (Fig. 24) after hardening. In addition, since the main component of the sand is SiO_2, higher SiO_2 diffraction peaks appear in all three modified MPC mortar samples. After fly ash or silica fume is mixed into MPC mortar two silicates, a series of hydration reactions may occur in the system(Chen & Lan, 2000; Haque et al., 2020), and Al_2SiO_5 and $MgSiO_3$, were also found in 10%FA-MPC and 15%SF-MPC. The formation of $MgSiO_3$ is attributed to hydrogen bonding association and dissociation of $Mg(OH)_2$ (Ruan et al., 2022). MgO is infiltrated by water molecules, its surface forms a complex $Mg(OH)_2$ due to hydrogen bond. The $Mg(OH)_2$ gradually decomposed into Mg_2^+ and OH^-, and Mg_2^+ and free SiO_3^{2-} eventually formed the complex $MgSiO_3$.

According to Table 12, among the three mineral materials, γ_1, the initial effect of metakaolin on the flexural strength of MPC mortar, is the largest, and $f_{\sigma f,t}$, the flexural strength time-growing coefficient, is still the largest after 28 days of curing. It can be proved by Fig. 24c, where MKP appears around the metakaolin particles and the crystal shape of its MKP is more irregular and the surface is rougher compared with 15% SF-MPC. This

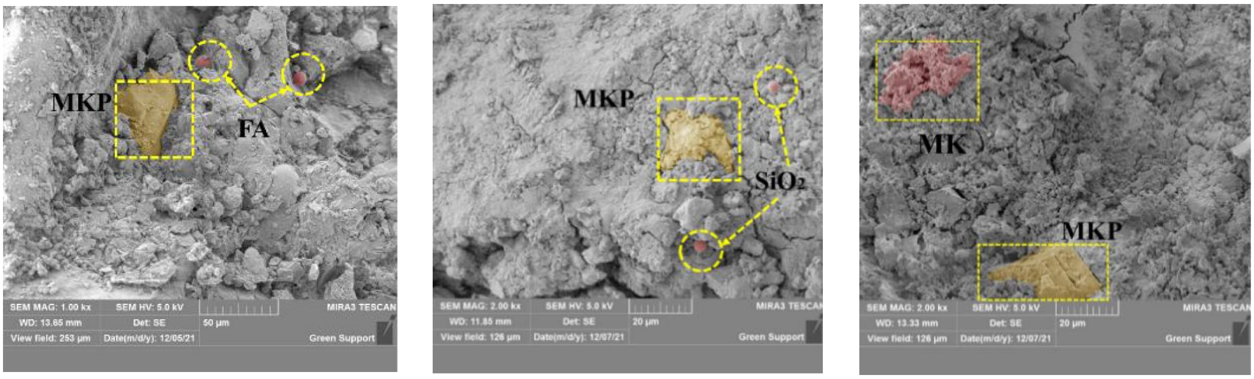

a. 10%FA-MPC b. 15%SF-MPC c. 10%MK-MPC

Fig. 24 SEM results of modified MPC mortar after air-curing for 28 days

may increase friction and bonding between the crystals inside the modified-MPC mortar, further explaining that metakaolin brings higher flexural strength. Meanwhile, in Table 12, γ_6, the initial effect of silica fume on the compressive strength of MPC mortar, is the largest while $f_{\sigma c,t}$, the compressive strength time-growing coefficient, is still the largest after 28 days of curing. 15% SF-MPC has fewer defects such as cracks and is denser microscopically compared to the remaining two groups. The reason is that spherical particles, SiO_2 in silica fume, of different sizes are clearly visible in Fig. 24b. The active SiO_2 act in the MPC system to fill the pores and react with the free state Mg^{2+} to produce $MgSiO_3$ and make MPC mortar specimens denser (Wang et al., 2020), improving the compressive strength of MPC mortar. The above mentioned also proves that 15% SF-MPC performs better in terms of compressive strength than other two MPC mortar.

10% FA-MPC is the only sample with a positive value for $f_{\sigma f,I}$, the flexural strength incorporation-growing coefficient. And $f_{\sigma c,I}$, the degradation of its compressive strength incorporation-growing, is also the smallest among the three samples. It means that for the 10% FA-MPC, the appropriate increase in incorporation can improve the flexural strength, which is proved by the relative more fly ash particles in the 10% FA-MPC (Fig. 24a). The strength of the MPC mortar is improved by the "ball" effect of FA (Liu & Chen, 2019), which increases the overall denseness of MKPC mortar by physical filling, and the more filled particles also reduce the effect of the fluctuation of the incorporation error. 15% SF-MPC obtains the maximum weakening coefficients $f_{\sigma f,I}$ and $f_{\sigma c,I}$ in terms of strength variation with incorporations. It indicates that small incorporation fluctuations of SF near its optimal incorporation can bring about large strength loss, so to ensure the optimal-incorporation SF-MPC strength should be accurately calculated and added with SF. To summarize, the fluctuation of the percentage of FA content near the optimal content will not cause a decrease in strength, and the accuracy of the required strength content is required to be low. The fluctuation of the percentage of SF near the optimal incorporation will cause a decrease in strength, therefore, high precision is required for the required incorporation of silica fume near the optimal incorporation.

In summary, among the three mineral materials, the best performance in terms of flexural strength of MPC mortar is the 10% incorporated metakaolin, and the best performance in terms of compressive strength is the 15% incorporated silica fume. The optimal incorporation of FA-MPC does not require high accuracy of FA incorporation, while SF-MPC requires high accuracy of SF incorporation, otherwise, it will cause large strength loss.

5 Conclusion

In this study, three mathematical models were used to model the relationship between mineral incorporations and curing time and the strength of modified MPC mortar based on strength tests, to achieve the evaluation of the effect of different minerals on the strength of modified MPC mortar and the prediction of the change of modified MPC mortar strength with mineral incorporations and curing time. And the effect of the different minerals was evaluated by the model with the best error performance combined with microscopic characterization, and the following conclusions were obtained:

(1) The strength test results showed that the 10% incorporated fly ash, 15% incorporated silica fume, and 10% incorporated metakaolin were the optimum incorporations. With cured in air for 28d, the flexural and compressive strength increases of 10% FA-

MPC were 1.6 MPa and 11.6 MPa, and the flexural and compressive strength increases of 15% SF-MPC were 2.5 MPa and 24.4 MPa, and the flexural and compressive strength increases of 10% MK-MPC were 2.3 MPa and 12.3 MPa. The best-performing minerals in improving the flexural and compressive strength of the modified MPC mortar were metakaolin and silica fume.

(2) The data distribution-shaped nonlinear model showed the best fitting error performance, which could better describe the trend of the strength data with incorporations and curing time, but also controlled the prediction error of the model for the strength of the three materials to less than 12.5%. This model's R^2 is mostly over 0.7, which means that it can more accurately represent 70% of the variations in strength with respect to incorporations and curing time, which was more in line with the actual situation.

(3) The Strength-DDSNM's shape provides a visual representation of how incorporations, curing time, and their interactions affect the strength of mineral-modified MPC. The strength typically rises and then falls with increasing incorporations when the cure time is established. Strength has a characteristic of rising swiftly at beginning, then slowing down as the curing period grows when the incorporations are constant. Regarding the interaction of the incorporations and curing time, on the one hand, the strength varies more noticeably as the curing time increases and the incorporations grow, on the other hand, the strength increases more quickly per unit of time when the incorporations are increased within a certain range.

(4) The strength influence coefficients of the three materials were calculated by the data distribution-shaped nonlinear model for 28 days of natural curing under their respective optimum incorporation, and their microscopic characterization was analyzed by combining XRD and SEM. 10% incorporated metakaolin with an initial flexural strength coefficient of 11.32 and a flexural strength time-growing coefficient of 0.0675 was the best material to improve the flexural strength of MPC mortar, which is because that crystal shape of MKP around the metakaolin particles shows more irregular and rougher the surface, increasing the friction and bonding between the crystals inside the modified-MPC mortar. 15% incorporated silica fume with an initial compressive strength coefficient of 31.37 and a compressive strength time-growing coefficient of 0.6076 was the best material to improve the compressive strength, because the active SiO_2 acts in the MPC system to fill the pores and react with the free state Mg^{2+} to produce $MgSiO_3$ and make MPC mortar specimens denser.

(5) The optimal-incorporation fly ash-modified MPC mortar does not require high accuracy of FA incorporation, while silica fume-modified MPC mortar requires high accuracy of SF incorporation, otherwise, it will cause large strength loss.

Acknowledgements
The work described in this paper was supported by the National Natural Science Foundation of China (No. 51978060) and Science and Technology Plan Project of Shaanxi Province (2023-YBGY-1 84). Thanks to the contribution from Zongbin Wang and Yizhuo Han for their devotion in the experiment and structure of the paper.

Author contributions
The authors confirm contribution to the paper as follows: study conception and design: YY and QK; data collection: RL and YZ; analysis and interpretation of results: QK and JB; draft manuscript preparation: QK and HH. Manuscript revision: QK, JB and YZ. All authors reviewed the results and approved the final version of the manuscript.

Funding
National Natural Science Foundation of China (No. 51978060); Science and Technology Plan Project of Shaanxi Province (2023-YBGY-1 84).

Availability of data and materials
All data generated or analyzed during this study are included in this published article and the data file could be offered by contacting the corresponding author if needed.

Declarations

Ethics approval and consent to participate
Not applicable.

Consent for publication
The manuscript is approved by all authors for publication. The author declares that the work described was original research that has not been published previously, and not under consideration for publication elsewhere, in whole or in part.

Competing interests
The authors declare that they have no known competing financial interests or personal relationships that could have appeared to influence the work reported in this paper.

Received: 25 September 2023 Accepted: 14 December 2023
Published online: 12 March 2024

References

Ahmad, M. R., & Chen, B. (2018). Effect of silica fume and basalt fiber on the mechanical properties and microstructure of magnesium phosphate cement (MPC) mortar. *Construction and Building Materials, 190*, 466–478.

Ahmad, M. R., Chen, B., & Jiang, Y. (2019). A comprehensive study of basalt fiber reinforced magnesium phosphate cement incorporating ultrafine fly ash. *Composites Part B: Engineering, 168*(19), 204–217.

Ahmadi, M., & Kioumarsi, M. (2023). Predicting the elastic modulus of normal and high strength concretes using hybrid ANN-PSO. *Materials Today: Proceedings*. https://doi.org/10.1016/j.matpr.2023.03.178

Bai, L., et al. (2023). Investigation of water stability and microcharacteristics of magnesium potassium phosphate cement modified by calcium

aluminate cement and wollastonite. *Construction and Building Materials., 369*, 130580.
Chau, C. K., Qiao, F., & Li, Z. (2011). Microstructure of magnesium potassium phosphate cement. *Construction and Building Materials., 25*(6), 2911–2917.
Chen, C. Y., Lan, G. S., et al. (2000). Preparation of mullite by the reaction sintering of kaolinite and alumina. *Journal of the European Ceramic Society, 20*(14–15), 2519–2525.
El-Jazairi, B. (1982). Rapid repair of concrete pavings. *Concrete, 16*, 9.
Fang, B., et al. (2003). Research progress on the properties and applications of magnesium phosphate cement. *Ceramics International, 49*(3), 4001–4016.
Gill, P. E., & Wong, E. (2012). *Sequential quadratic programming methods. Mixed integer nonlinear programming* (pp. 147–224). New York: Springer.
Haque, M. A., Chen, B., & Liu, Y. (2020). The role of bauxite and fly-ash on the water stability and microstructural densification of magnesium phosphate cement composites. *Construction and Building Materials, 260*, 119953.
Hawkins, D. M. (2004). The problem of overfitting. *Journal of Chemical Information and Computer Sciences., 44*(1), 1–12.
Hu, M., et al. (2008). A note on cubic polynomial interpolation. *Computers & Mathematics with Applications, 56*(5), 1358–1363.
Huete-Hernández, S., et al. (2021). Fabrication of sustainable magnesium phosphate cement micromortar using design of experiments statistical modelling: Valorization of ceramic-stone-porcelain containing waste as filler. *Ceramics International, 47*(8), 10905–10917.
IBM SPSS. (2013). *Statistics for Windows, version 24*. New York: IBM Corp.
Jiang, Yu. (2019). Muhammad Riaz Ahmad, and Bing Chen. Properties of magnesium phosphate cement containing steel slag powder. *Construction and Building Materials, 195*, 140–147.
Liao, W., et al. (2017). Potential large-volume beneficial use of low-grade fly ash in magnesia-phosphate cement based materials. *Fuel, 209*, 490–497.
Liu, Y., & Chen, B. (2019). Research on the preparation and properties of a novel grouting material based on magnesium phosphate cement. *Construction and Building Materials, 214*, 516–526.
Lv, L., et al. (2019). Properties of magnesium potassium phosphate cement pastes exposed to water curing: A comparison study on the influences of fly ash and metakaolin. *Construction and Building Materials, 203*, 589–600.
Ma, C., et al. (2021). Effect of early-hydration behavior on rheological properties of borax-admixed magnesium phosphate cement.". *Construction and Building Materials, 283*, 122701.
Ma, C., et al. (2022). Influencing mechanism of silica fume on early-age properties of magnesium phosphate cement-based coating for hydraulic structure. *Journal of Building Engineering, 54*, 104623.
Mahmood, W., et al. (2022). Interpreting the experimental results of compressive strength of hand-mixed cement-grouted sands using various mathematical approaches. *Archives of Civil and Mechanical Engineering, 22*(1), 1–25.
MathWorks. (2016). *MATLAB*. Natick: MathWorks.
Mohammed, A., Salih, A., & Raof, H. (2020). *Vipulanandan constitutive models to predict the rheological properties and stress-strain behavior of cement grouts modified with metakaolin*. Pennsylvania: ASTM International.
Qin, Z., et al. (2020). Effects of metakaolin on properties and microstructure of magnesium phosphate cement. *Construction and Building Materials, 234*, 117353.
Ruan, S. (2022). Life cycle assessment of different alternative materials used for stabilization/solidification. *Low Carbon Stabilization and Solidification of Hazardous Wastes*. https://doi.org/10.1016/B978-0-12-824004-5.00002-53
Ruan, W., Li, F., Liao, J., et al. (2022). Effects of water purifying material waste on properties and hydration mechanism of magnesium phosphate cement-based grouting materials. *Construction and Building Materials, 349*, 128676.
Runqing, L., et al. (2023). Static and dynamic mechanical properties of magnesium phosphate cement modified by metakaolin after high-temperature treatment. *Construction and Building Materials, 392*, 131933.
Sattarifard, A. R., et al. (2022). Fresh and hardened-state properties of hybrid fiber–reinforced high-strength self-compacting cementitious composites. *Construction and Building Materials, 318*, 125874.
Sun, Z., et al. (2023). Feasibility of high-magnesium nickel slag-fly ash as precursor of magnesium phosphate cement and its hydration mechanism. *Construction and Building Materials, 401*, 132880.
The State Bureau of Quality and Technical Supervision. (2021a). *Code for Test method of cement mortar strength (ISO method)*. Beijng: The State Bureau of Quality and Technical Supervision.
The State Bureau of Quality and Technical Supervision. (2021b). *Method of testing cements-Determination of strength*. Beijing: The State Bureau of Quality and Technical Supervision.
Vipulanandan, C., & Mohammed, A. (2018). Smart cement compressive piezoresistive, stress-strain, and strength behavior with nanosilica modification. *Journal of Testing and Evaluation, 47*(2), 1479–1501.
Walling, S. A., & Provis, J. L. (2016). Magnesia-based cements: A journey of 150 years, and cements for the future? *Chemical Reviews, 116*(7), 4170–4204.
Wang, D., et al. (2023). Effect of magnesium-to-phosphate ratio on the corrosion resistance of magnesium alloy embedded in magnesium potassium phosphate cement. *Cement and Concrete Composites, 135*, 104826.
Wang, Q., Wu, Z. H., Zhang, G. L., et al. (2020). Volumetric stability and hydration properties of magnesium silicate cementitious materials. *Journal of Silicates, 48*(05), 682–688.
Xie, Y., et al. (2020). Preliminary investigation of the hydration mechanism of MgO-SiO2-K_2HPO_4 cement. *Construction and Building Materials, 235*, 117471.
Yang, N., et al. (2014). Research progresses in magnesium phosphate cement–based materials. *Journal of Materials in Civil Engineering, 26*(10), 04014071.
Yasar, A., Bilgili, M., & Simsek, E. (2012). Water demand forecasting based on stepwise multiple nonlinear regression analysis. *Arabian Journal for Science and Engineering, 37*(8), 2333–2341.
Yue, Y, et al. (2016). A statistical investigation of the rheological properties of magnesium phosphate cement. International Workshop on Innovation in Low-carbon Cement & Concrete Technology
Zhang, J., et al. (2023). Experimental research on mechanical properties and microstructure of magnesium phosphate cement-based high-strength concrete. *Journal of Building Engineering, 65*, 105784.
Zhou, X., et al. (2019). Experimental investigation and mathematical strength model study on the mechanical properties of cemented paste backfill. *Construction and Building Materials, 226*, 524–533.

Publisher's Note

Qi Kang Master student; School of Civil Engineering, Chang an University, Xi an 710061 China

Jingxin Bao Undergraduate student; Chang'an Dublin International College of Transportation, Chang'an University, Xi'an 710061 China

Ran Li Master student; School of Civil Engineering, Chang'an University, Xi'an 710061, China

Yingying Zuo Master student; School of Civil Engineering, Chang'an University, Xi'an 710061, China

Yanxia Ye Professor: School of Civil Engineering, Chang'an University, Xi'an 710061, China

Hua Huang Professor; School of Civil & Architecture Engineering. Xi'an Technological University, Xi'an 710061, China